Small-scale turbulence; theory, phenomenology and applications

Large-eddy simulation with stretched-vortex SGS model

D.I. Pullin

Graduate Aeronautical Laboratories

California Institute of Technology

Cargèse, August 20, 2007

Carlos Pantano, David Hill, Ralf Deiterding, Daniel Chung

Overview

- LES of compressible, shock-driven turbulence
  - *Extension of SGS model to compressible flow*
  - *Issues of numerical methodology*
  - *Adaptive Mesh Refinement (AMR)*

- LES of Richtmyer-Meshkov instability with re-shock
  - *Growth of mixing layer thickness*
  - *Resolved-scale turbulence statistics*
  - *Multi-scale modeling; subgrid extension of turbulence statistics*
  - *Effect of magnetic field*
  - *Cylindrical RM instability*

- Near-wall SGS modeling
  - *No large eddies near the wall*
  - *Local inner scaling and near-wall modeling*
  - *Virtual-wall model*
  - *LES of channel flow at large Re_\tau*

Favre-filtered Navier-Stokes equations

$$\frac{\partial\overline{\rho}}{\partial t} + \frac{\partial\overline{\rho}\tilde{u}_j}{\partial x_j} = 0$$

$$\frac{\partial\overline{\rho}\tilde{u}_i}{\partial t} + \frac{\partial(\overline{\rho}\tilde{u}_i\tilde{u}_j + \overline{p}\delta_{ij})}{\partial x_j} = \frac{\partial\sigma_{ij}}{\partial x_j} - \frac{\partial\tau_{ij}}{\partial x_j}$$

$$\frac{\partial\overline{E}}{\partial t} + \frac{\partial(\overline{E}+\overline{p})\tilde{u}_j}{\partial x_j} = \frac{\partial}{\partial x_j}\left(\overline{\kappa}\frac{\partial\overline{T}}{\partial x_j}\right) + \frac{\partial\sigma_{ji}\tilde{u}_i}{\partial x_j} - \frac{\partial q_j^T}{\partial x_j}$$

$$\frac{\partial\overline{\rho}\tilde{\psi}}{\partial t} + \frac{\partial(\overline{\rho}\tilde{\psi}\tilde{u}_j)}{\partial x_j} = \frac{\partial}{\partial x_j}\left(\overline{\rho}\tilde{D}\frac{\partial\tilde{\psi}}{\partial x_j}\right) - \frac{\partial q_j^\psi}{\partial x_j}$$

$$\begin{aligned}\tau_{ij} &= \overline{\rho}(\widetilde{u_i u_j} - \tilde{u}_i\tilde{u}_j)\\ q_j^T &= \overline{\rho}(\widetilde{c_p T u_j} - \tilde{c}_p\tilde{T}\tilde{u}_j)\\ q_j^\psi &= \overline{\rho}(\widetilde{\psi u_j} - \tilde{\psi}\tilde{u}_j)\end{aligned}$$

$$\overline{E} = \frac{\overline{p}}{(\tilde{\gamma}-1)} + \frac{1}{2}\overline{\rho}(\tilde{u}_k\tilde{u}_k) + \frac{1}{2}\tau_{kk}$$

$$\overline{p} = \frac{\overline{\rho}R\tilde{T}}{\tilde{m}}$$

- Two-component Favre-filtered NS equations
- Filtering procedure strictly formal
  - *Not performed explicitly in LES*
  - *Guide to SGS modeling*
- Favre-filtered quantities identified with resolved-scale quantities in LES
  - *Modeling assumption on par with SGS modeling*
- Model subgrid flux of temperature as a passive scalar

LES of compressible turbulence. LES and strong shocks (D. Hill). Hybrid WENO-TCDS algorithm:

- Numerical methods for shock-capturing and LES `orthogonal'.
- Our solution: hybrid technique: blending Weighted Essentially Non-Oscillatory (WENO) scheme with Tuned Centered-Difference (TCD) stencil.
- WENO in regions of very-large density ratio (Shocks)
  - *But WENO is not suitable for LES in smooth regions away from shocks.*
  - *Upwinding strategy is too dissipative*
- TCD stencil in smooth regions away from shocks
  - *Low numerical dissipation (centered method)*
  - *optimized for minimum resolved-scale discretization error in LES (Ghosal, 1996)*
  - *5- or 7-point stencil trades off formal order of accuracy for small dispersion errors*
- Target WENO stencil = TCD stencil
- In practice, target TCD stencil not always achieved; switch is used based on acceptable WENO smoothness measure
- Hybrid method designed for LES in presence of strong shocks

SAMR and AMROC (R. Deiterding)

- Structured Adaptive Mesh Refinement (SAMR)
- Adaptive Mesh Refinement Object Oriented C++ (AMROC)
- Berger & Colella's algorithm for conservation laws of the form:

$$\frac{\partial \boldsymbol{q}}{\partial t} + \frac{\partial}{\partial x_k}\boldsymbol{f}^k(\boldsymbol{q}) = 0,$$

- Hierarchical data structure contains the solution vector and fluxes
- On each patch, a standard Cartesian fluid solver is applied to march the solution (e.g. WENO/TCD)
- Boundary conditions and synchronization between patches is accomplished by filling ghost cells with interpolated data.
  - *ghost cell interpolation is an approximation for non-linear systems of equations*

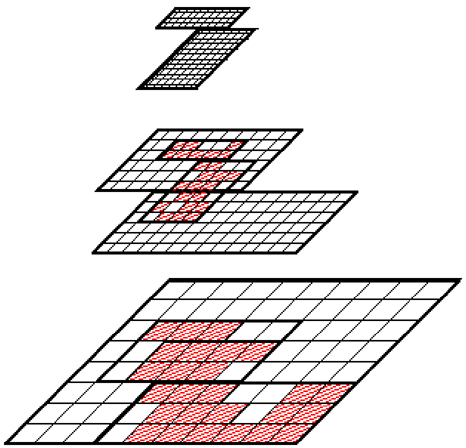

Figure 1. AMR hierarchy.

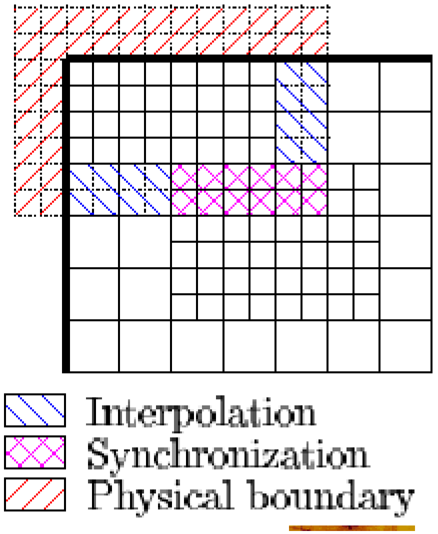

Richtmyer-Meshkov (R-M) Instability

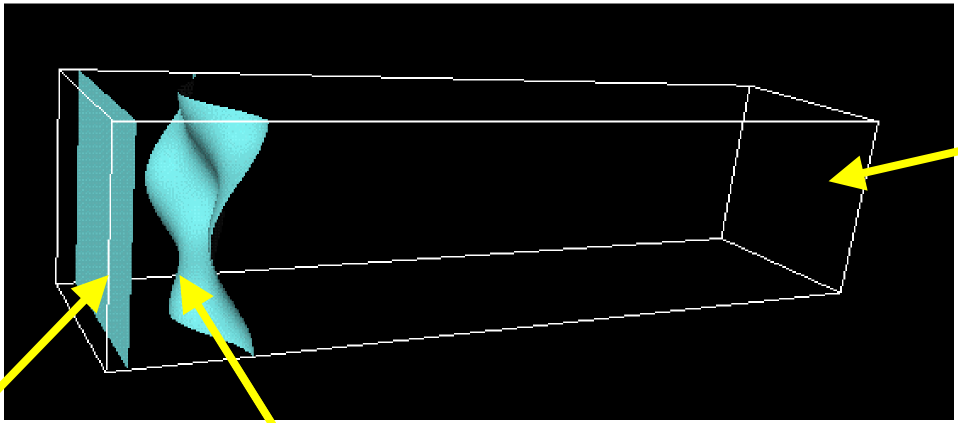

Shock reflects off end

Incident shock

interface

Misalignment of contact and shock

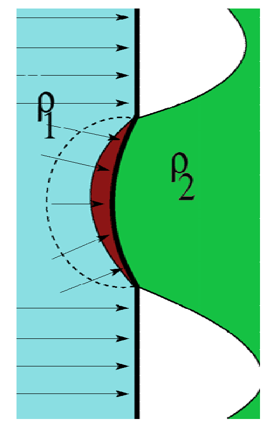

Self-stretching and dilitation

Barotropic vorticity Generation

$$\frac{\partial \varpi}{\partial t} + u \bullet \nabla \varpi = \varpi \bullet \nabla u - \varpi \nabla \bullet u + \frac{1}{\rho^2} \nabla(\rho) \times \nabla(p)$$

Advection

Richtmyer-Meshkov (R-M) Instability

- Astrophysics: A role in the description of the explosion of supernovae (Smarr 1981, Arnett 1989.)
  - *Supernova 1987A R. McCray (JILA) Images from HST*

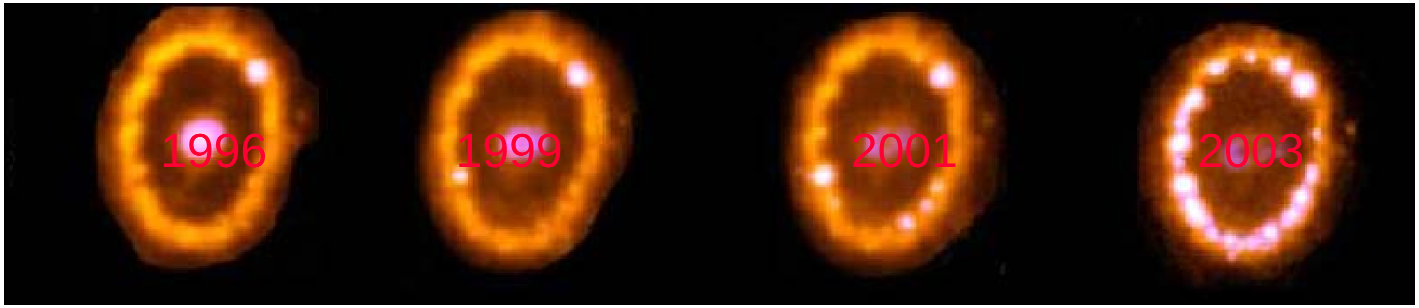

- A role in Inertial confinement fusion design (Lund 1997)
  - *Laser pulse drives pressure waves*
- Canonical example of shock-turbulence interaction

Flow Description

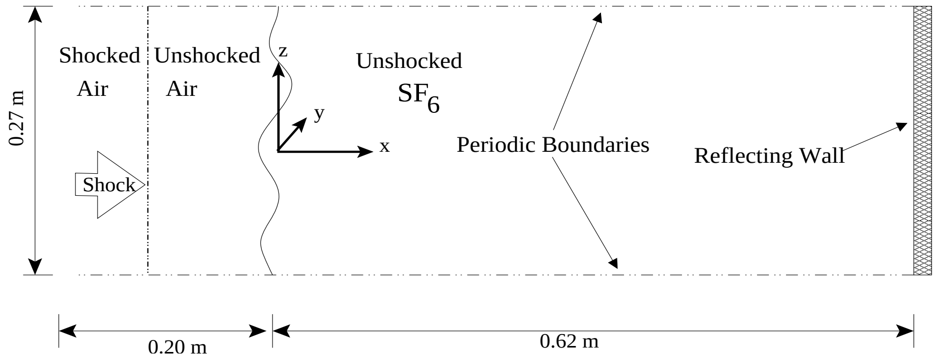

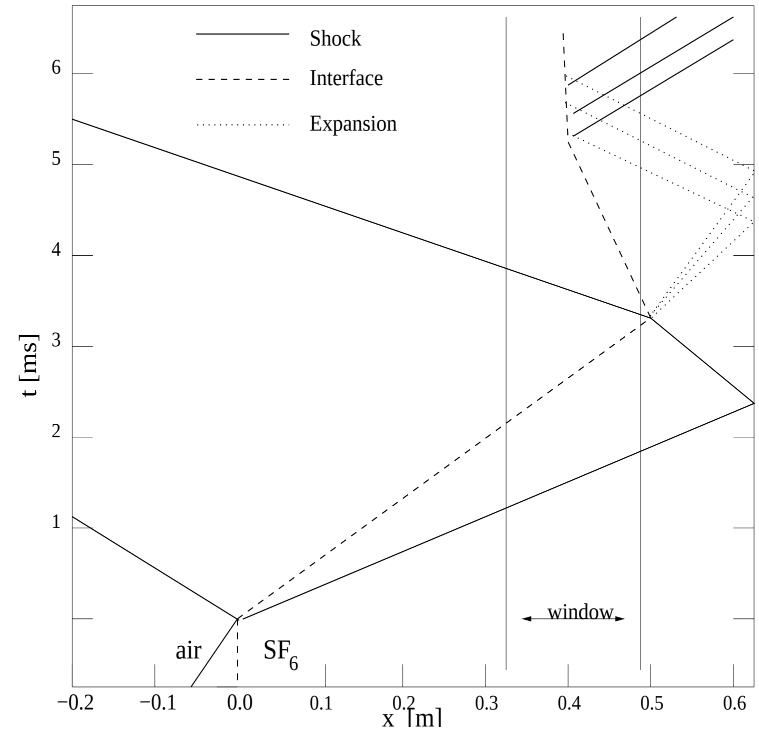

	II^b	VI^b	VII^b
Incident Mach number	1.24	1.50	1.98
Pressure (kPa)	40	23	8
Length, membrane to end wall (cm)	110	62	49
Instantaneous velocity (ms^{-1})	72	150	287
Shocked growth rate (ms^{-1})	2.1	4.2	7.5
Reshocked growth rate (ms^{-1})	17.0	37.2	74.4
Shocked observation times (ms)	4.7-6.7	2.2-3.2	1.7-2.5
Reshocked observation times (ms)	15.5-16.5	4.0-5.5	1.7-2.5

Table 1: The test conditions and growth rates of the interface thickness from Vetter & Sturtevant (1995).

Shock tube, flow conditions (Vetter & Sturtevant 1995)
and 1-D wave diagram

2D-Richtmyer-Meshkov (R-M) Instability

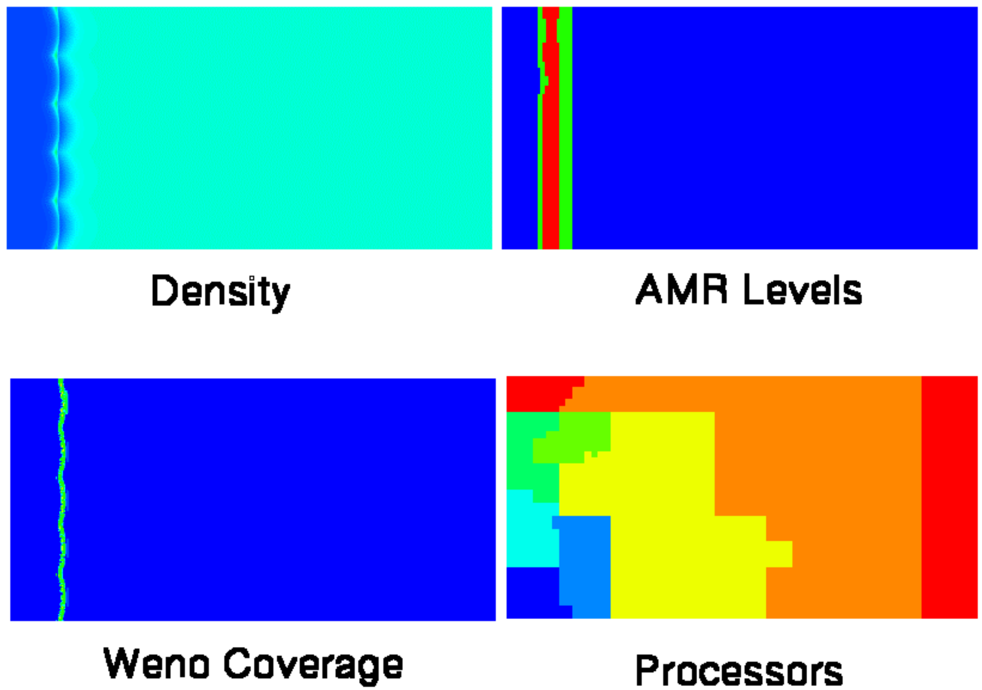

Computational runs: unigrid

- Unigrid simulations
- QSC supercomputer (Los Alamos)

	II^b	VI^b	VI^e	VII^b
Incident Mach number	1.24	1.50	1.50	1.98
Computational grid	$616\mathrm{x}128^2$	$388\mathrm{x}128^2$	$776\mathrm{x}256^2$	$327\mathrm{x}128^2$
Computational resolution: $\triangle x$ (cm)	0.21	0.21	0.105	0.21
Simulation time (ms)	16.62	6.35	12.0	2.57
CPU hours	3,982	972	38,400	544

Table 1: The computational cost in CPU hours for each of the runs. Simulation VI^e is a higher resolution version of VI^b computed to about twice the experimental time.

LES of planar Richtmyer-Meshkov instability

- Vetter & Sturtevant (1995) RMI with reshock off end wall
- Air/SF_6, Mach=1.5
- 3 levels of refinement

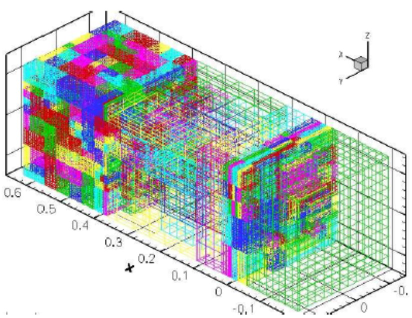

Mesh at one time

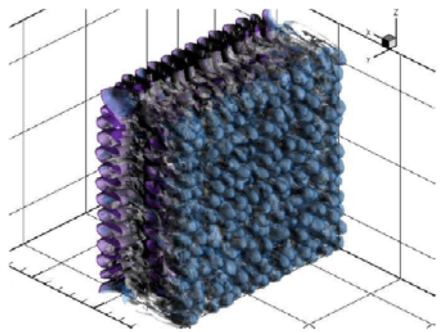

Interface at one time

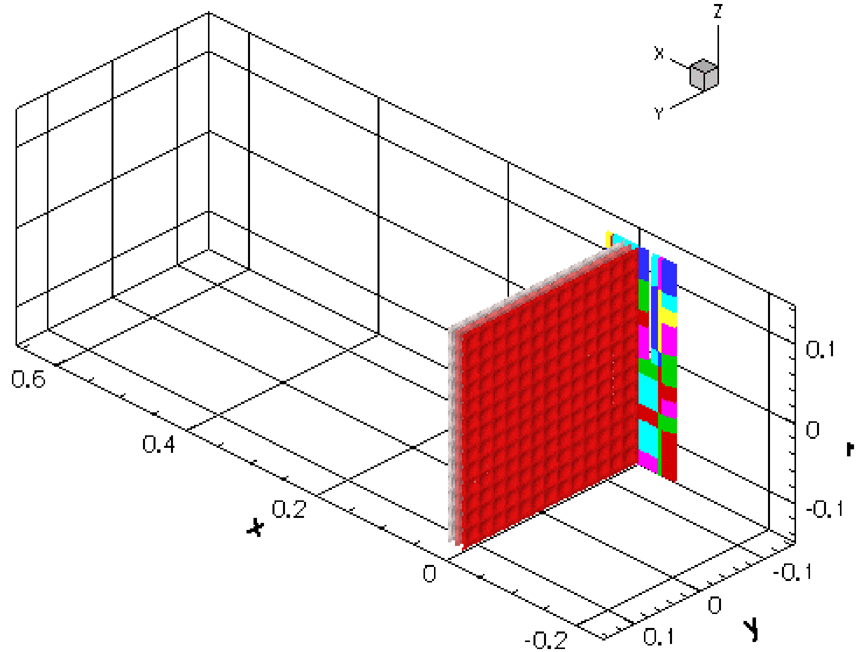

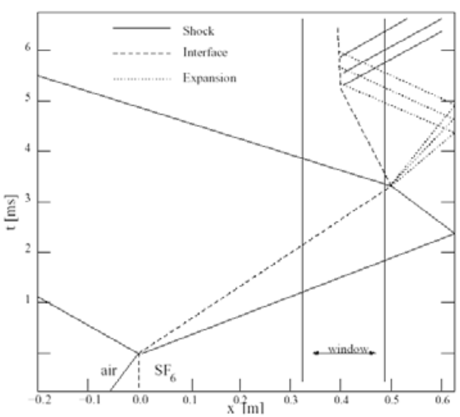

Wave diagram

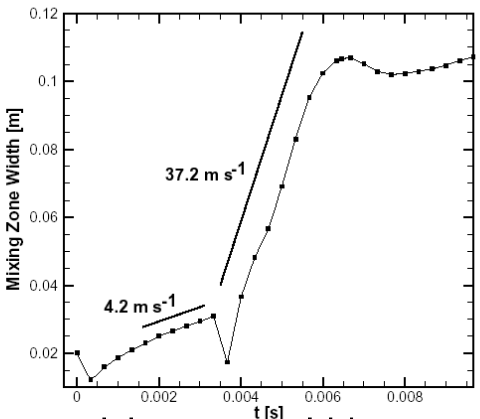

Mixing zone width

LES of planar R-M instability;

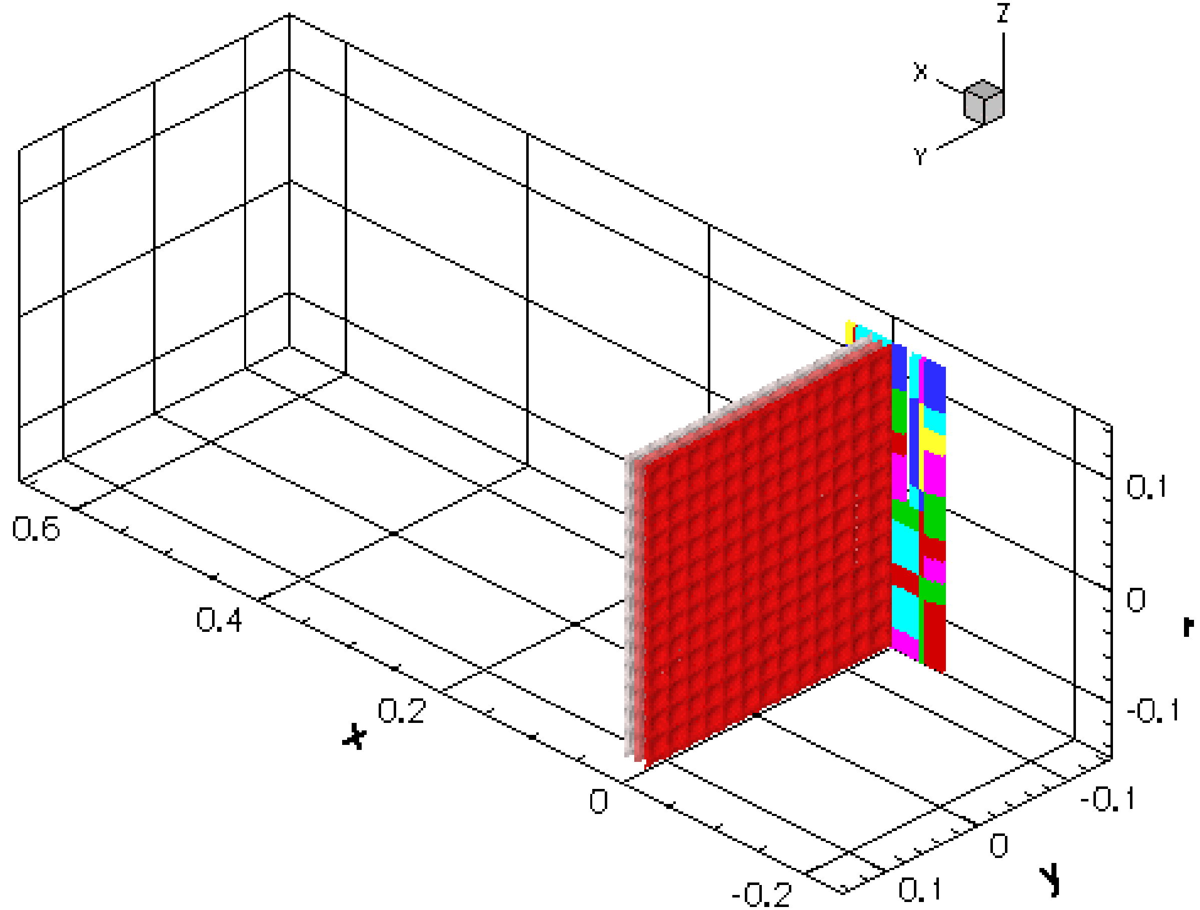

- Vetter Sturtevant (1995) RMI with reshock off end wall
- Air/SF_6, Mach=1.5
- 3 levels of refinement

Growth of turbulent mixing zone

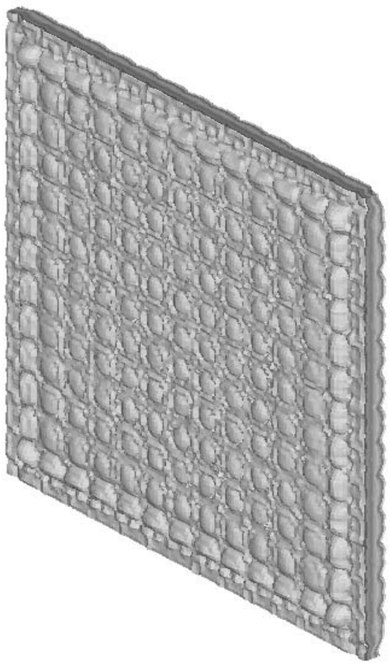

T = 0. ms

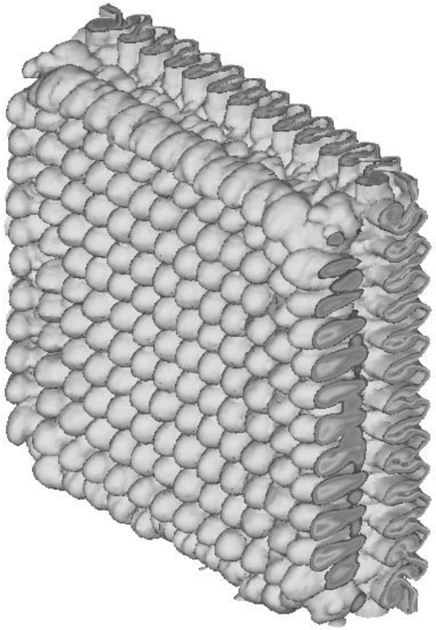

T = 3.6 ms

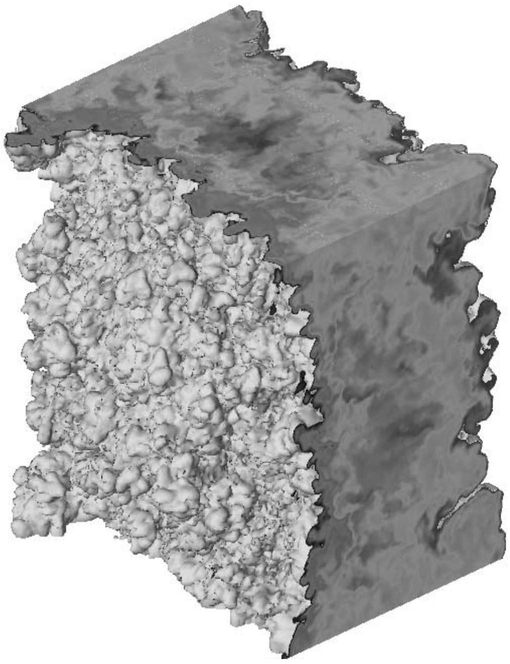

T = 10.0 ms

Growth of turbulent mixing zone

y-z plane-averaged mixing-layer width
compared with Vetter & Sturtevant (1995)

$$\langle f(x,t)\rangle = \frac{1}{\mathcal{A}}\int\int f(x,y,z,t)\,dydz$$

$$\delta_{\mathrm{MZ}}(t) = 4\int_{\mathrm{tube}}(1-\langle\psi\rangle)\langle\psi\rangle dx$$

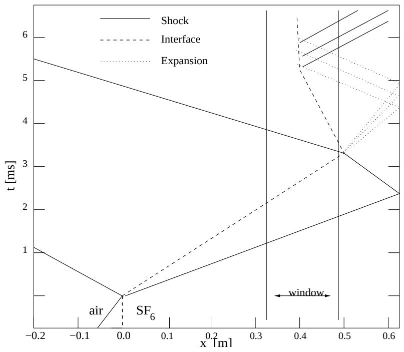

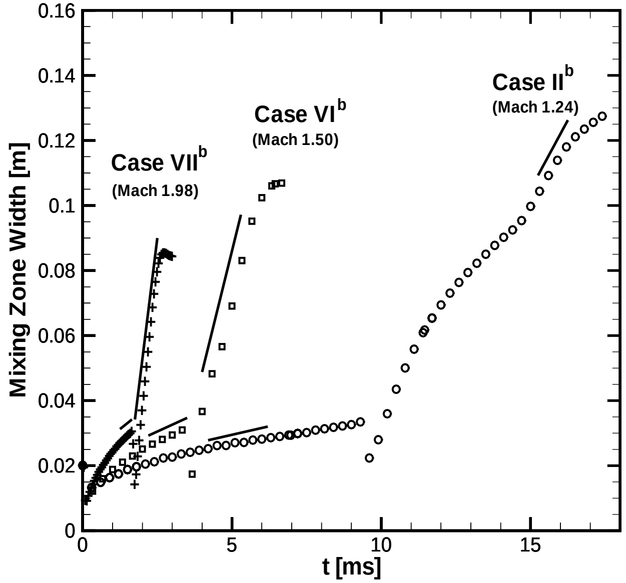

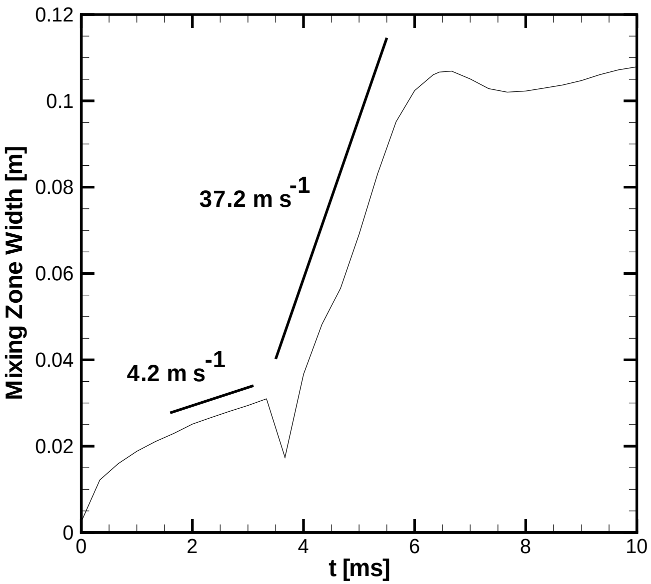

Case VIe; 776x256x256

Kinetic energy in mixing layer

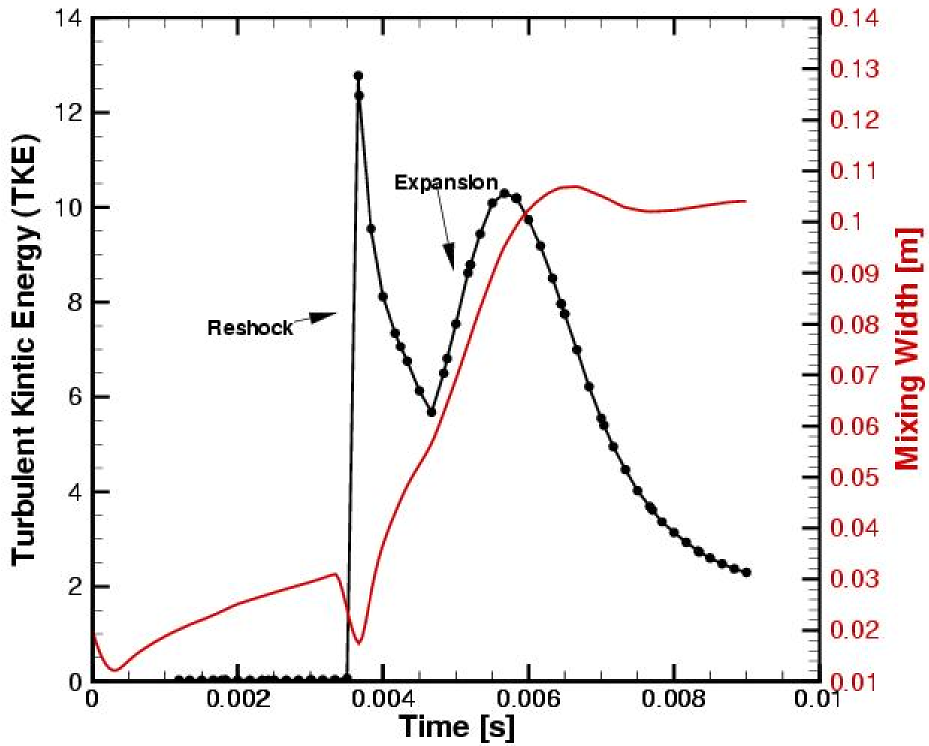

Resolved-scale radial spectra in y-z plane

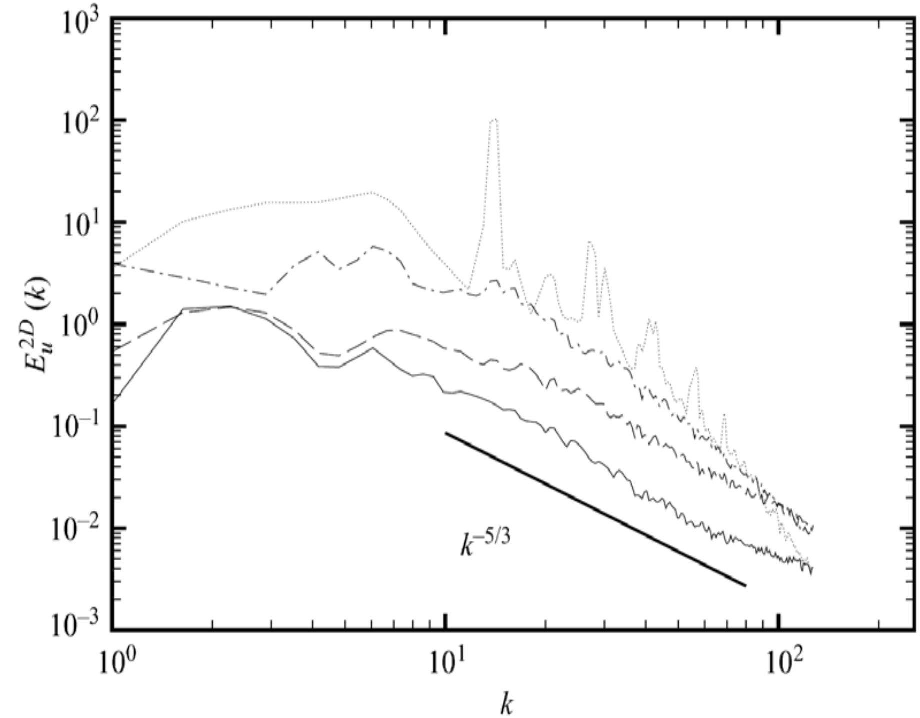

FIGURE 12. Radial power spectra of velocity $E_u^{2D}(k)$ computed in the centre plane of the TMZ at four different times: $t = 4.5$ ms (dotted line), $t = 6.5$ ms (dashed-dot line), $t = 7.6$ ms (dashed line) and $t = 10$ ms (solid line). All computed wavenumbers shown and $k_{max} = 128$.

Resolved-scale radial spectra in y-z plane

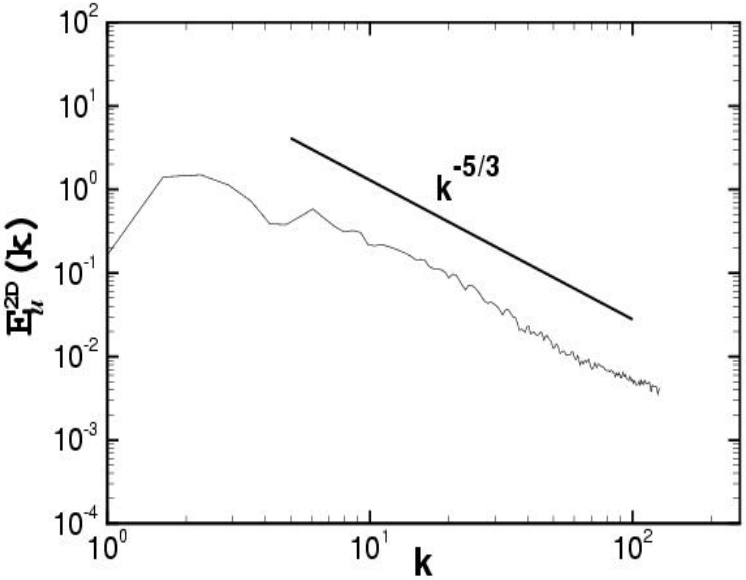

Radial spectrum of x-velocity, center of mixing layer

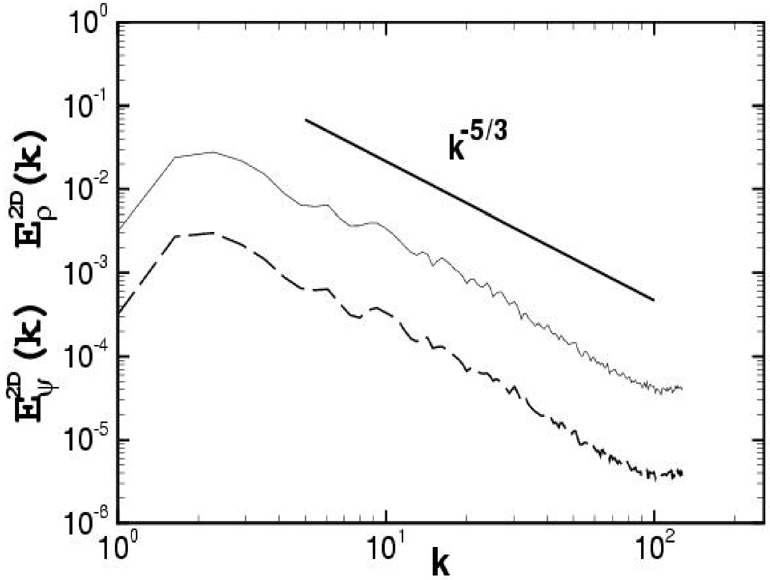

Radial spectrum of density (solid) and mixture fraction, center of mixing layer

Subgrid continuation

- Stretched-spiral vortex SGS model used for subgrid continuation
  - *Contains description of local anisotropy*
  - *Computation of local and plane-averaged Kolmogorov scale η*
  - *Parameters computed from LES (structure functions)*

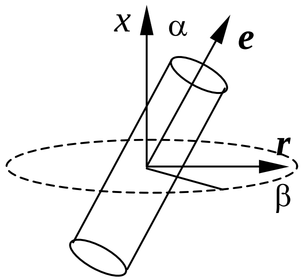

$$E(k) = \mathcal{K}_0 \epsilon^{2/3} k^{-5/3} \exp[-2k^2\nu/(3|\tilde{a}|)]$$

$$\tilde{a} = \tilde{S}_{ij} e_i^v e_j^v, \qquad \tilde{S}_{ij} = \frac{1}{2}\left(\frac{\partial \tilde{u}_i}{\partial x_j} + \frac{\partial \tilde{u}_j}{\partial x_i}\right)$$

$$E_{qq}^{2D}(k_r, \alpha_0) = \frac{2k_r}{\pi}\int_{k_r}^{|k_r/\cos\alpha_o|} \frac{E(\kappa)}{(\kappa^2 - k_r^2)^{1/2}(k_r^2 - \kappa^2\cos^2\alpha_o)^{1/2}} d\kappa.$$

$$E_{33}^{2D}(k_r, \alpha_0) = \frac{2k_r}{\pi}\int_{k_r}^{|k_r/\cos\alpha_o|} \frac{(k_r^2 - \kappa^2\cos^2\alpha_o)^{1/2} E(\kappa)}{\kappa^2(\kappa^2 - k_r^2)^{1/2}} d\kappa.$$

Subgrid continuation of radial velocity spectra

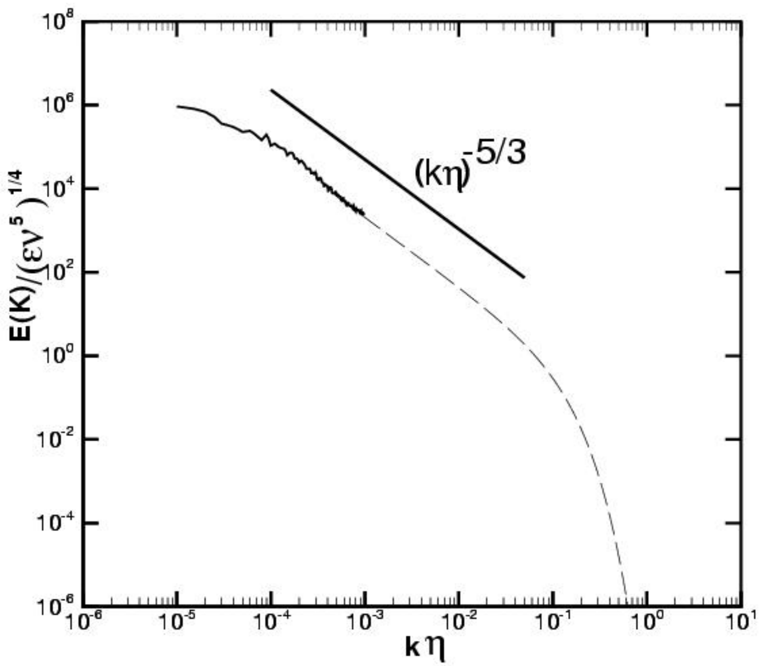

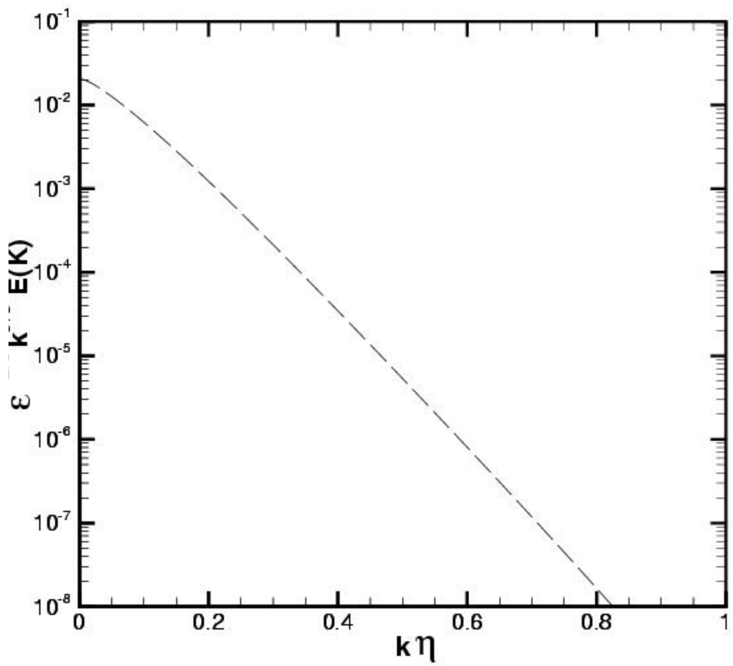

- Radial (in k-space) velocity spectrum on center plane of mixing layer
  - *Resolved-scale spectrum (solid)*
  - *Subgrid continuation (dashed)*
  - *Parameters computed from LES (structure functions)*
- Subgrid velocity spectrum in dissipation range
  - *Log-linear scale*
  - *Note exponential roll-off*

Subgrid continuation of radial velocity spectra.
Anisotropy of in-plane and normal velocity spectra

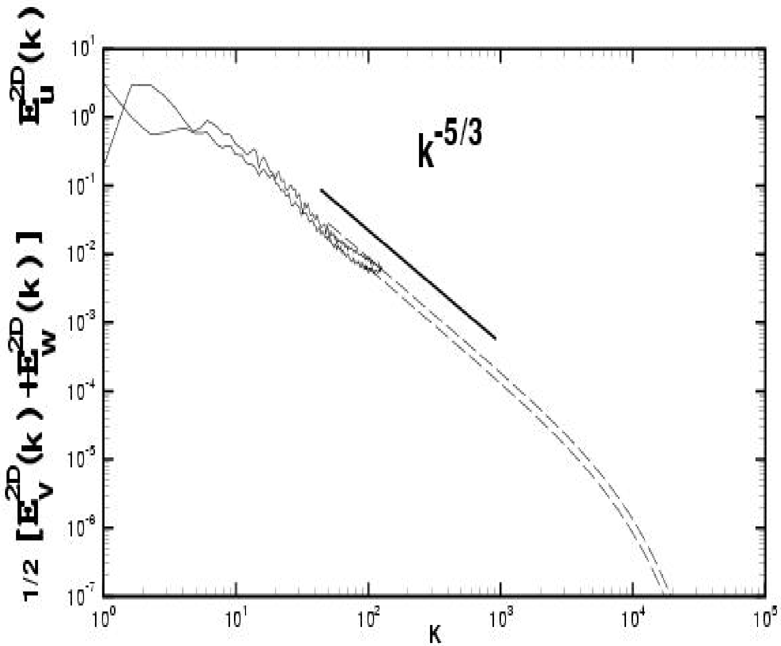

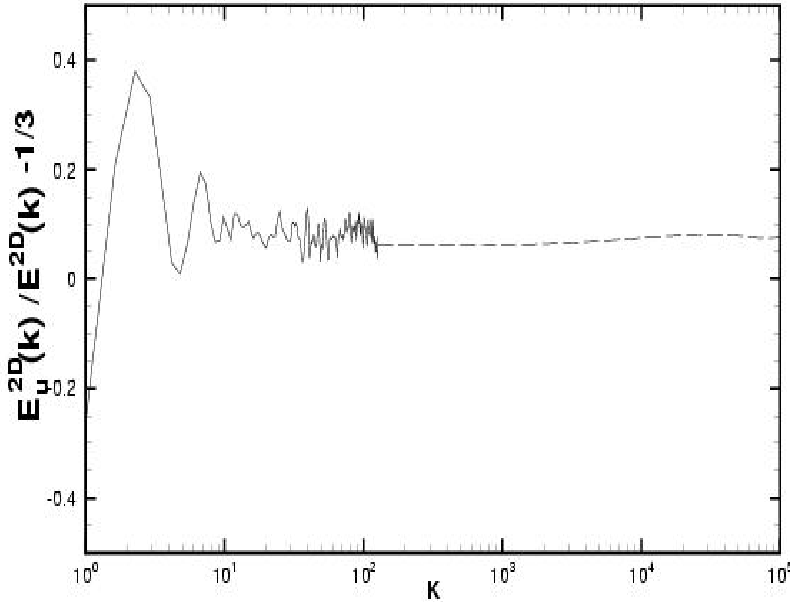

- Radial spectrum of u (top) and u+w (below)
  - *Resolved-scale spectrum (solid)*
  - *Subgrid continuation (dashed)*

- Measure of anisotropy for radial velocity spectra
  - *Resolved-scale spectrum (solid)*
  - *Subgrid continuation (dashed)*

Subgrid continuation of scalar spectum in y-z plane

Scalar spectrum for stretched-spiral vortex

Pullin & Lundgren (2000)

$$E_\psi(k) = \mathcal{K}_\psi \left(k^{-5/3} \exp(-\frac{(4\nu + 2D)k^2}{3\tilde{a}}) + \frac{8}{5\pi} \left(\frac{2\Gamma}{\tilde{a}}\right)^{1/3} k^{-1} \exp(-\frac{2Dk^2}{3\tilde{a}}) \right)$$

$$\tilde{\mathcal{F}}_2^\psi(\triangle) = 4\mathcal{K}_\psi \triangle^{2/3} \int_0^\pi \left(s^{-5/3} + \frac{8}{5\pi} \left(\frac{2\Gamma}{\tilde{a}\triangle^2}\right)^{1/3} s^{-1} \right) \left(1 - \frac{\sin s}{s}\right) ds$$

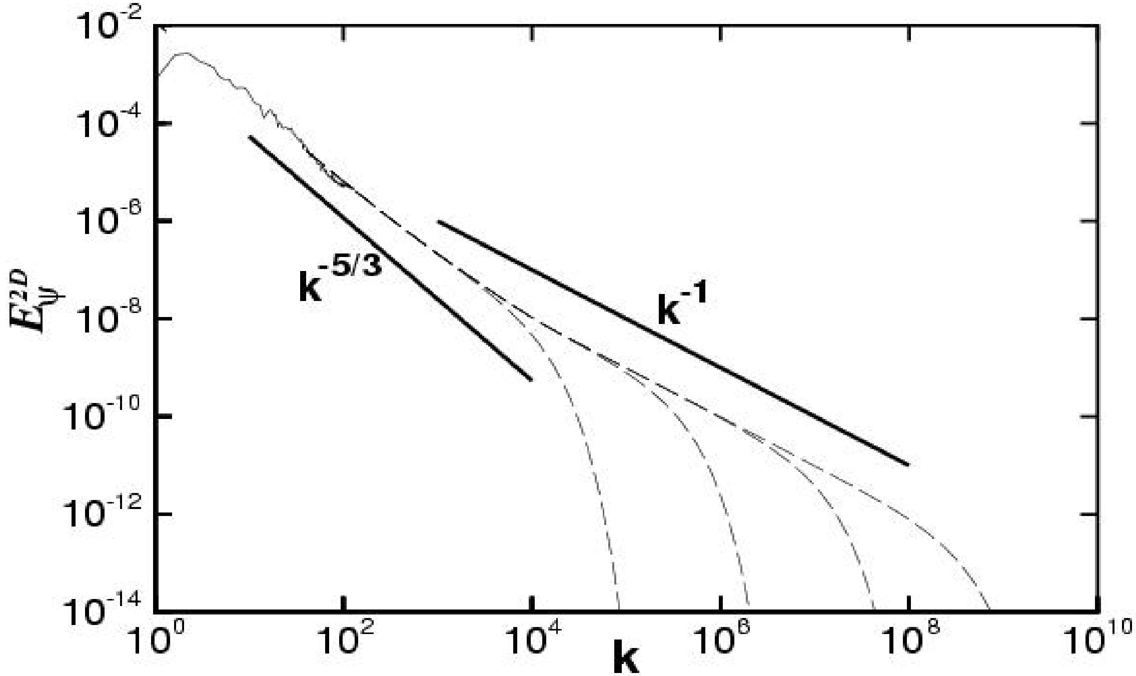

Resolved-scale and continued scalar spectrum in center y-z plane, t = 10ms. Left to right, Sc = 1, 1000, 1000,000

P.D.F. of mixture fraction with subgrid correction

$$\tilde{\mathcal{P}}_{sgs}(\psi,\tilde{\psi},\sigma^2_\psi;\boldsymbol{x},t) = \tilde{\mathcal{P}}_{sgs}(\psi|\tilde{\psi},\sigma^2_\psi)\tilde{\mathcal{P}}_{sgs}(\tilde{\psi},\sigma^2_\psi;\boldsymbol{x},t)$$

$$\tilde{\mathcal{P}}_{sgs}(\psi;\boldsymbol{x},t) = \int\int \tilde{\mathcal{P}}_{sgs}(\psi|\tilde{\psi},\sigma^2_\psi)\tilde{\mathcal{P}}_{sgs}(\tilde{\psi},\sigma^2_\psi;\boldsymbol{x},t)\, d\tilde{\psi} d\sigma^2_\psi$$

$$\tilde{\mathrm{P}}(\psi;\boldsymbol{x},t) \simeq \frac{\langle\overline{\rho}\tilde{\mathcal{P}}_{sgs}(\psi;\boldsymbol{x},t)\rangle}{\langle\overline{\rho}(\boldsymbol{x},t)\rangle}$$

$$\tilde{\mathcal{P}}_{sgs}(\psi;\boldsymbol{x},t) = \frac{\Gamma(a+b)}{\Gamma(a)\Gamma(b)}\psi^{a-1}(1-\psi)^{b-1}$$

$$a = \tilde{\psi}[\tilde{\psi}(1-\tilde{\psi})\sigma_\psi^{-2} - 1], \qquad b = a(\tilde{\psi}^{-1} - 1)$$

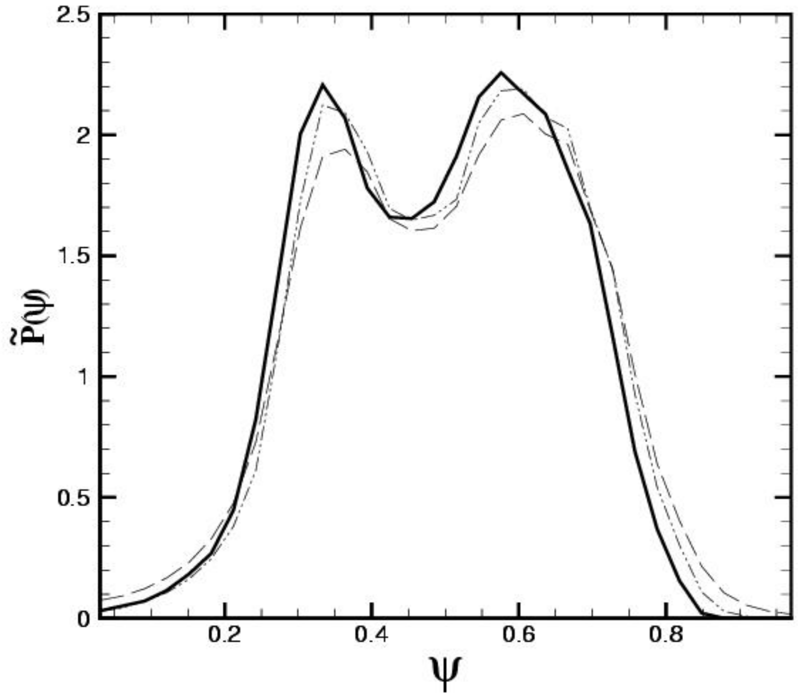

P.D.F of mixture fraction in center y-z plane, t = 10ms. Resolved-scale and Sc = 1, 1000,000

Suppression of RM instability by Magnetic Field
(V. Wheatley, R. Samtaney)

- Suppression due to change in shock refraction process at interface when $B \neq 0$ (Wheatley, Pullin & Samtaney, JFM 2004)
- Linear initial-value problem for impulsive acceleration of interface in presence of magnetic field solved exactly

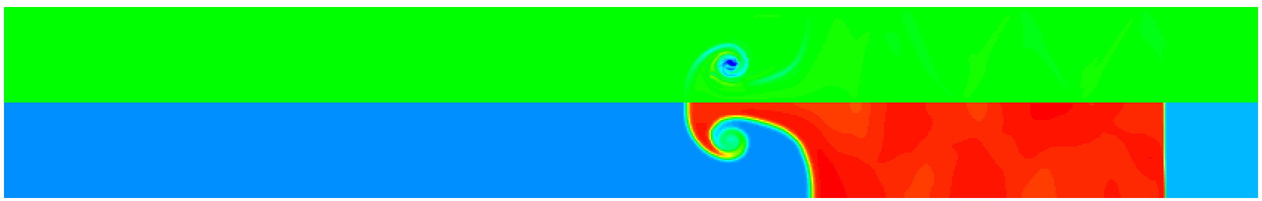

Vorticity (top) and ρ (bottom) at t =1.8 , B = 0, interface unstable

Vorticity (top) and ρ (bottom) at t =1.8, $B \neq 0$, instability suppressed

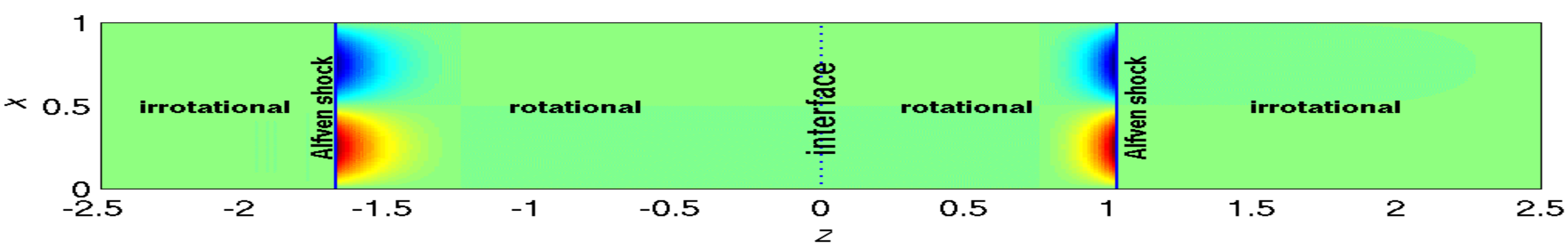

Analysis: Solution Features: PRL, 2005

Solution consists of:

- Inner region of rotational flow
- 2 small amplitude Alfvén shocks that carry circulation
- 2 outer irrotational regions

Notes:

- $w^*(0, t)$ is interfacial growth rate
- this decays to zero as Alfvén shocks propagate away

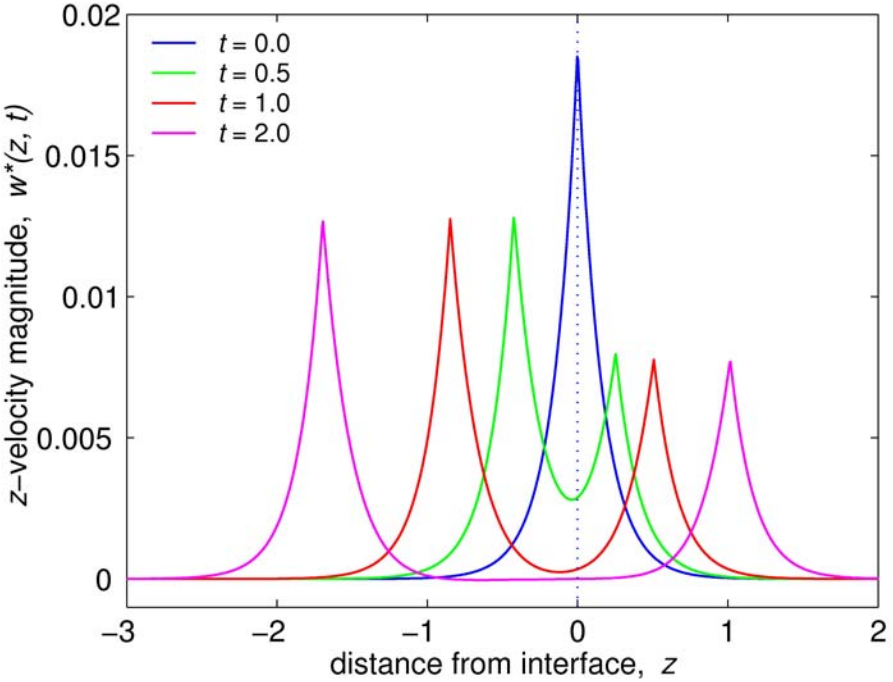

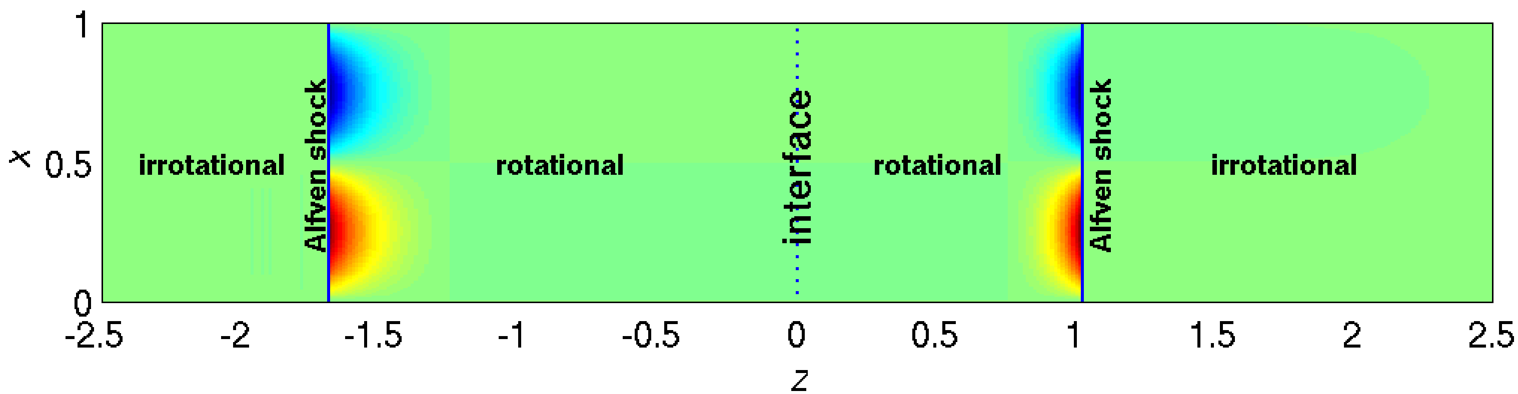

Cylindrical RMI: Flow Description

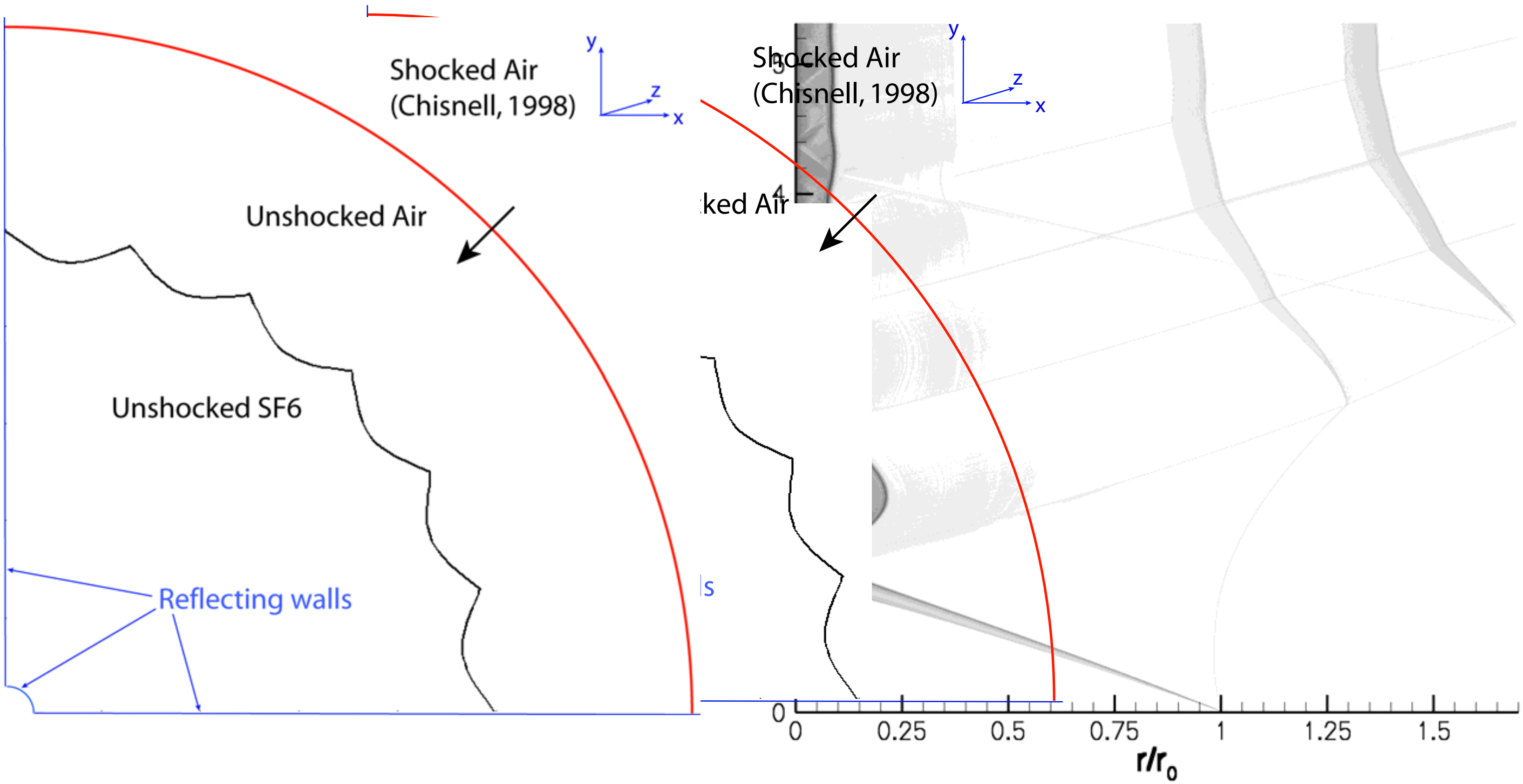

Flow conditions and 1-D wave diagram (*r*,*t*)

Cylindrical RMI; M_0=1.3, 90 degree wedge (M. Lombardini)

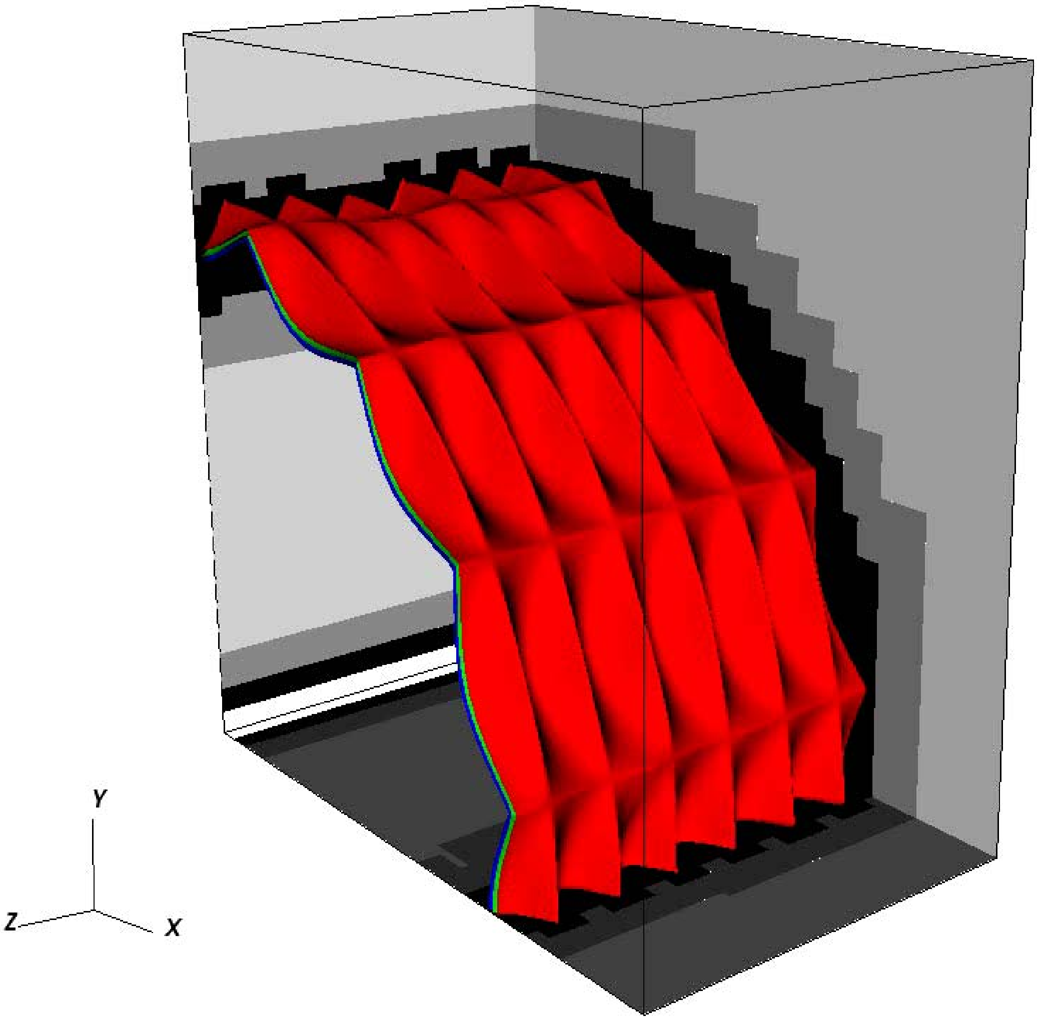

- WENO-TCD with LES (SV model)
- Adaptive Mesh Refinement (AMROC) Ghost Fluid Method (inner and outer cylindrical boundaries)
- Initial conditions:
  - *M_0 = 1.3 or 2.0 or 3.0*
  - *Air/SF_6 (Atwood number = 2/3)*
  - *"egg-carton" + smaller symmetry breaking perturbation with random phase*
  - *Chisnell's converging flow behind the shock wave*
- Resolution:
  - *Base grid 83 x 83 x 51*
  - *2 additional levels of refinement*
  - *Equivalent refined resolution 332 x 332 x 204*

Passive scalar contours & adaptive levels of refinement

Growth of turbulent mixing zone (M_0=2.0)

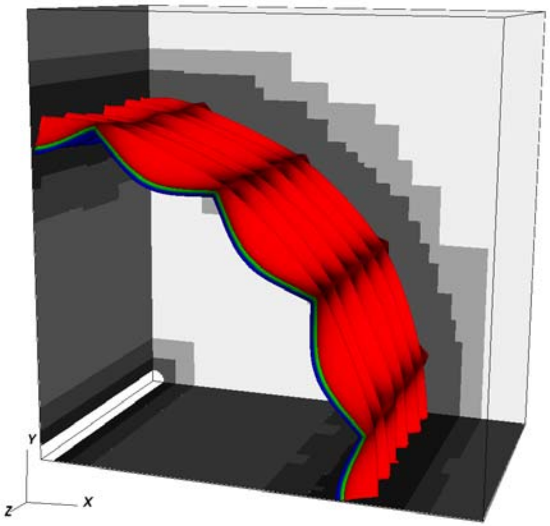

t = 0. ms

Initial condition

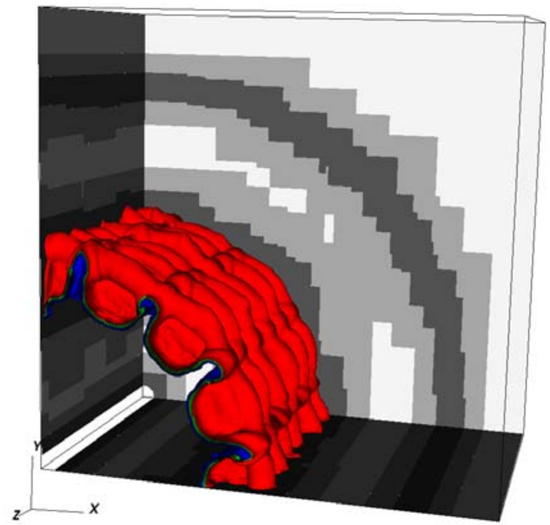

t = 1.45 ms

After first shock interaction

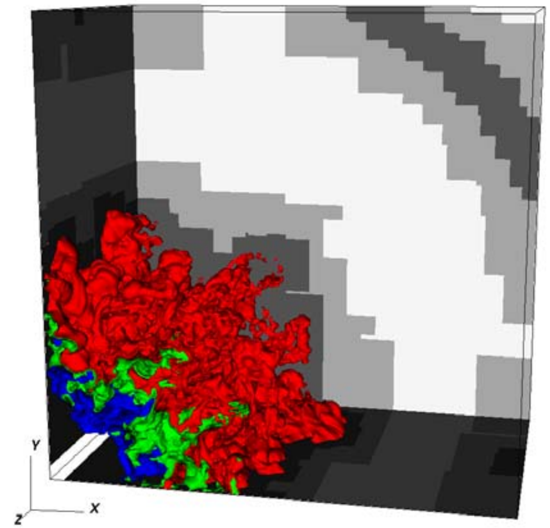

t = 5.13 ms

After first reschock

Turbulent channel flow (work in progress)

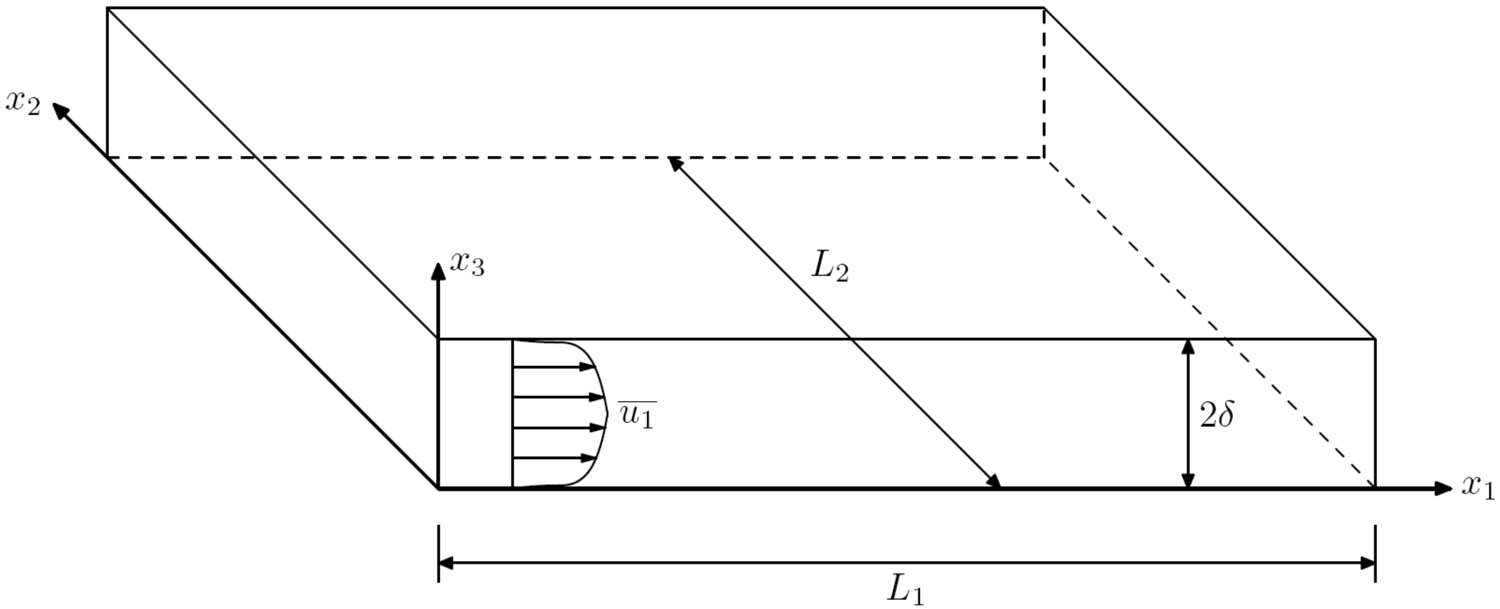

$$-\delta \overline{\frac{\partial p}{\partial x_1}} = \nu \left(\frac{\partial \overline{u_1}}{\partial x_3} \right)_{\text{wall}} \equiv u_\tau^2, \qquad \mathrm{Re}_\tau = u_\tau \delta / \nu$$

No large eddies near wall

Ten questions concerning the large-eddy simulation of turbulent flows

Stephen B Pope
Sibley School of Mechanical and Aerospace Engineering, Cornell University, Ithaca, NY 14853, USA
E-mail: pope@mae.cornell.edu

New Journal of Physics **6** (2004) 35
Received 3 December 2003
Published 16 March 2004
Online at http://www.njp.org/ (DOI: 10.1088/1367-2630/6/1/035)

A second example is high Reynolds number near-wall flows, the simplest specific case being the turbulent boundary layer on a smooth wall. The wall shear stress—all-important in aerodynamic applications—arises from momentum transfer from the outer flow through the boundary layer to the wall. In the viscous near-wall region, the momentum transfer is effected by the near-wall structures, the length scale of which scales with the tiny viscous length scale. As Bradshaw has succinctly put it: in the viscous near-wall region *there are no large eddies.* But, as has been appreciated at least since Chapman [15], the near-wall motions cannot be resolved in high-Reynolds number LES, but must instead be modelled (to avoid impracticable computational requirements that increase as a power of Reynolds number, as in DNS).

Near-wall filtering

Streamwise and spanwise Gaussian filter

$$\widetilde{Q}\left(x_1, x_2, x_3, t\right) \equiv \int_{-\infty}^{\infty} \int_{-\infty}^{\infty} Q\left(x_1', x_2', x_3, t\right) G_1\left(x_1, x_1'; \Delta_1\right) G_2\left(x_2, x_2'; \Delta_2\right)\, dx_1'\, dx_2'$$

$$\Delta_1, \Delta_2 \gg \nu / u_\tau$$

Wall-normal top-hat filter

$$\langle Q \rangle \left(x_1, x_2, t\right) \equiv \frac{1}{h} \int_0^h \widetilde{Q}\left(x_1, x_2, x_3', t\right)\, dx_3'$$

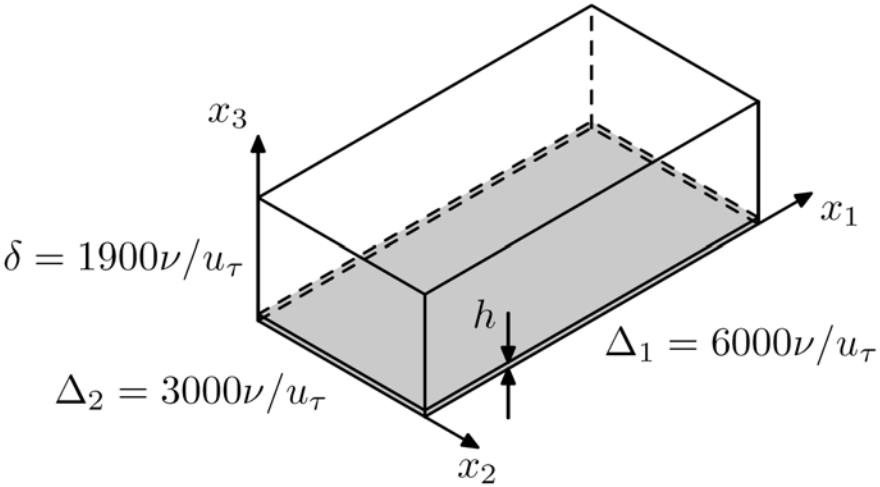

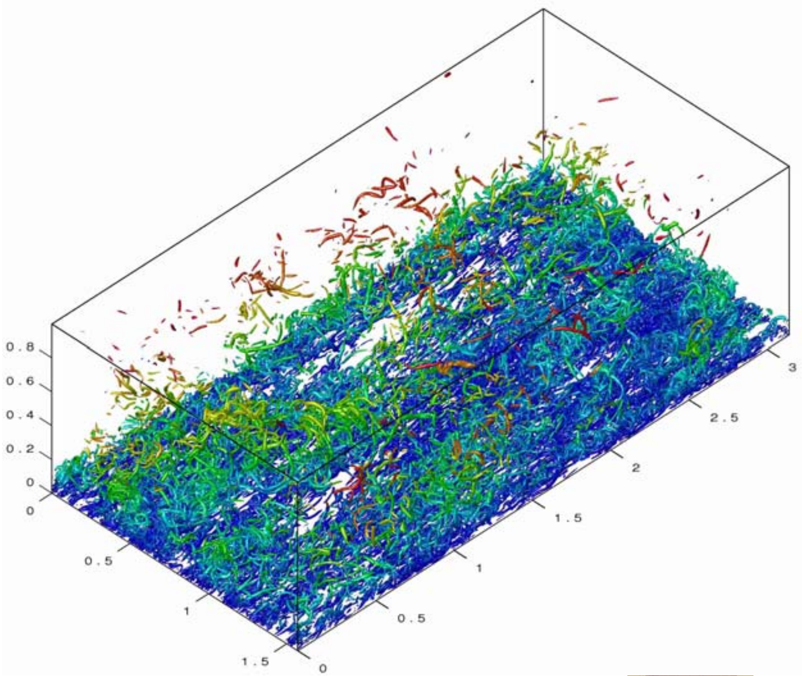

http://torroja.dmt.upm.es/ftp/channels/

Local inner scaling

Filtered streamwise momentum equation

$$\frac{\partial \langle u_1 \rangle}{\partial t} = \left(-\frac{1}{h}\widetilde{u_3 u_1} - \frac{\partial \widetilde{p}}{\partial x_1} + \frac{\nu}{h}\left[\frac{\partial \widetilde{u_1}}{\partial x_3} - u_0' \right] \right)_{x_3=h}$$

$$u_0' \left(x_1, x_2, t \right) \equiv \left(\frac{\partial \widetilde{u_1}}{\partial x_3} \right)_{x_3=0} = \widetilde{u_\tau}^2 \left(x_1, x_2, t \right) / \nu$$

Law of the wall in a local sense

$$\widetilde{u_1}^+ = F\left(x_3^+ \right) \quad \Longleftrightarrow \quad \frac{\widetilde{u_1}\left(x_1, x_2, x_3, t \right)}{\left(\nu u_0' \right)^{1/2}} = F\left(\frac{x_3}{\left(\nu / u_0' \right)^{1/2}} \right)$$

$$\frac{\partial \langle u_1 \rangle}{\partial t} = \frac{\left(\widetilde{u_1} \right)_{x_3=h}}{2\, u_0'} \frac{\partial u_0'}{\partial t}$$

Local shear stress equation

$$\frac{\partial u_0'}{\partial t} = \frac{2\, u_0'}{\left(\widetilde{u_1} \right)_{x_3=h}} \left(-\frac{1}{h}\widetilde{u_3 u_1} - \frac{\partial \widetilde{p}}{\partial x_1} + \frac{\nu}{h}\left[\frac{\partial \widetilde{u_1}}{\partial x_3} - u_0' \right] \right)_{x_3=h}$$

Fluctuating virtual-wall BC

$$\widetilde{u_1}^+(x_1, x_2, h_0, t) = F\left(h_0^+\right) = h_0^+, \quad h_0^+ \leq 10$$

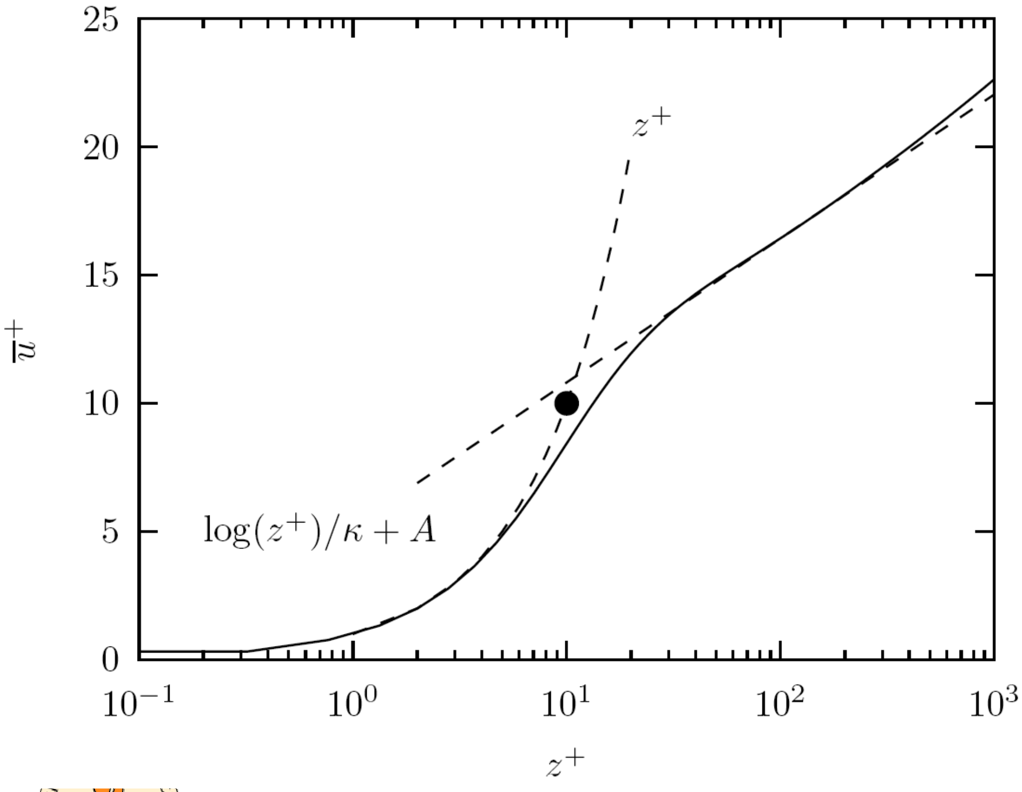

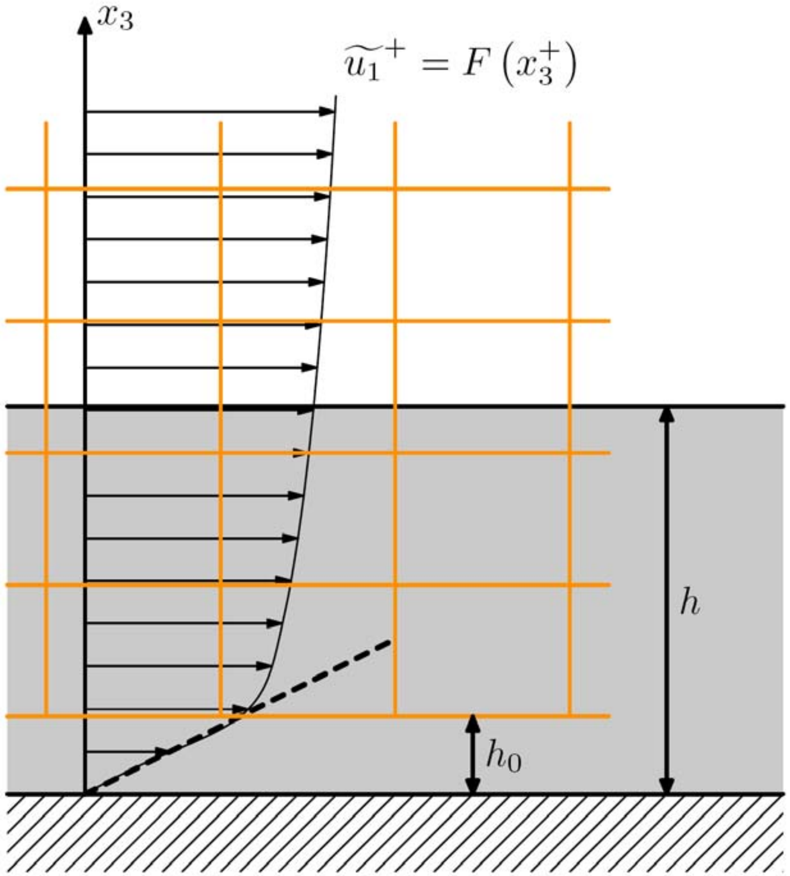

Extended stretched-vortex SGS model

LES decomposition

$$u_i(\mathbf{x},t) = \widetilde{U_i}(\mathbf{x},t) + U_i(\mathbf{x},t)$$

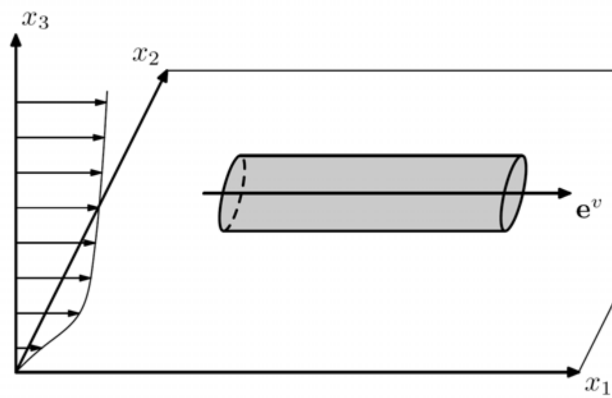

Dynamic alignment of subgrid vortices

$$\frac{\partial e_i^v}{\partial t} = e_j^v \frac{\partial \widetilde{U_i}}{\partial x_j} - e_i^v e_k^v e_j^v \frac{\partial \widetilde{U_k}}{\partial x_j}$$

Additional stresses from subgrid stretched-vortex wrapping axial velocity.

Pullin, D. I. & Lundgren, T. S. 2001 Axial motion and scalar transport in stretched spiral vortices. Phys. Fluids 13 (9), 2553-2563.

$$\begin{aligned} T_{ij} &= \widetilde{U_i U_j} + \widetilde{U_i \widetilde{U_j}} + \widetilde{\widetilde{U_i} U_j} \\ &= K\left(\delta_{ij} - e_i^v e_j^v\right) - \gamma \frac{1}{2}\Delta_c K^{1/2}\left(e_j^v e_k^v \frac{\partial \widetilde{U_k}}{\partial x_l}\left(\delta_{li} - e_l^v e_i^v\right) + e_i^v e_k^v \frac{\partial \widetilde{U_k}}{\partial x_l}\left(\delta_{lj} - e_l^v e_j^v\right)\right) \end{aligned}$$

$$\left(e_1^v, e_2^v, e_3^v\right) = (1,0,0) \quad \Rightarrow \quad T_{13} = -\gamma \frac{1}{2}\Delta_c K^{1/2} \frac{\partial \widetilde{U_1}}{\partial x_3}$$

LES coupled to wall closure

1) Time march local shear stress equation.

$$\frac{\partial u_0'}{\partial t} = \frac{2\,u_0'}{\left(\widetilde{u_1}\right)_{x_3=h}} \left(-\frac{1}{h}\widetilde{u_3 u_1} - \frac{\partial \widetilde{p}}{\partial x_1} + \frac{\nu}{h}\left[\frac{\partial \widetilde{u_1}}{\partial x_3} - u_0'\right]\right)_{x_3=h}$$

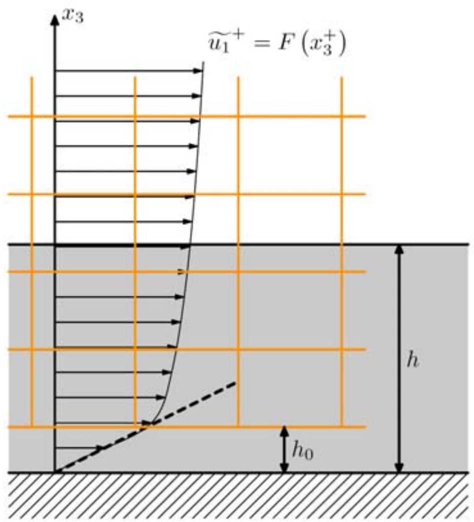

2) Obtain fluctuating slip BC from shear stress.

$$\widetilde{u_1}^+ \left(x_1, x_2, h_0, t\right) = F\left(h_0^+\right) = h_0^+, \quad h_0^+ \le 10$$

3) Time march filtered N-S with extended SGS model.

$$\begin{aligned} T_{ij} &= \widetilde{U_i U_j} + \widetilde{U_i \widetilde{U_j}} + \widetilde{\widetilde{U_i} U_j} \\ &= K\left(\delta_{ij} - e_i^v e_j^v\right) - \gamma \frac{1}{2}\Delta_c K^{1/2} \left(e_j^v e_k^v \frac{\partial \widetilde{U_k}}{\partial x_l}\left(\delta_{li} - e_l^v e_i^v\right) + e_i^v e_k^v \frac{\partial \widetilde{U_k}}{\partial x_l}\left(\delta_{lj} - e_l^v e_j^v\right)\right) \end{aligned}$$

4) Time march dynamic subgrid vortex alignment model.

$$\frac{\partial e_i^v}{\partial t} = e_j^v \frac{\partial \widetilde{U_i}}{\partial x_j} - e_i^v e_k^v e_j^v \frac{\partial \widetilde{U_k}}{\partial x_j}$$

Results (Re_{tau} = 600 to 60k)

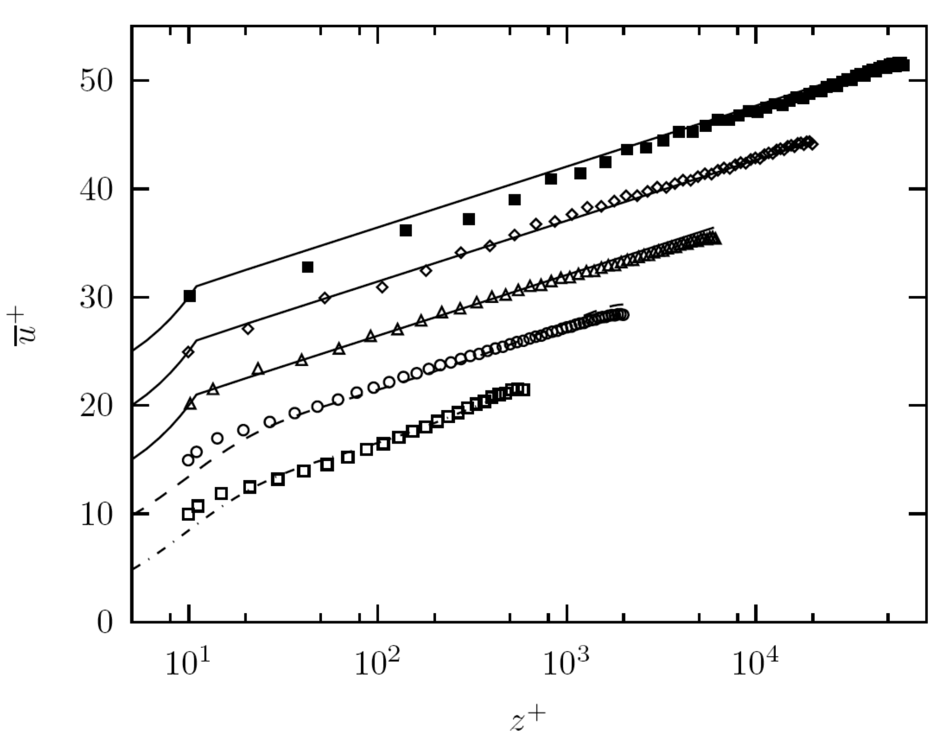

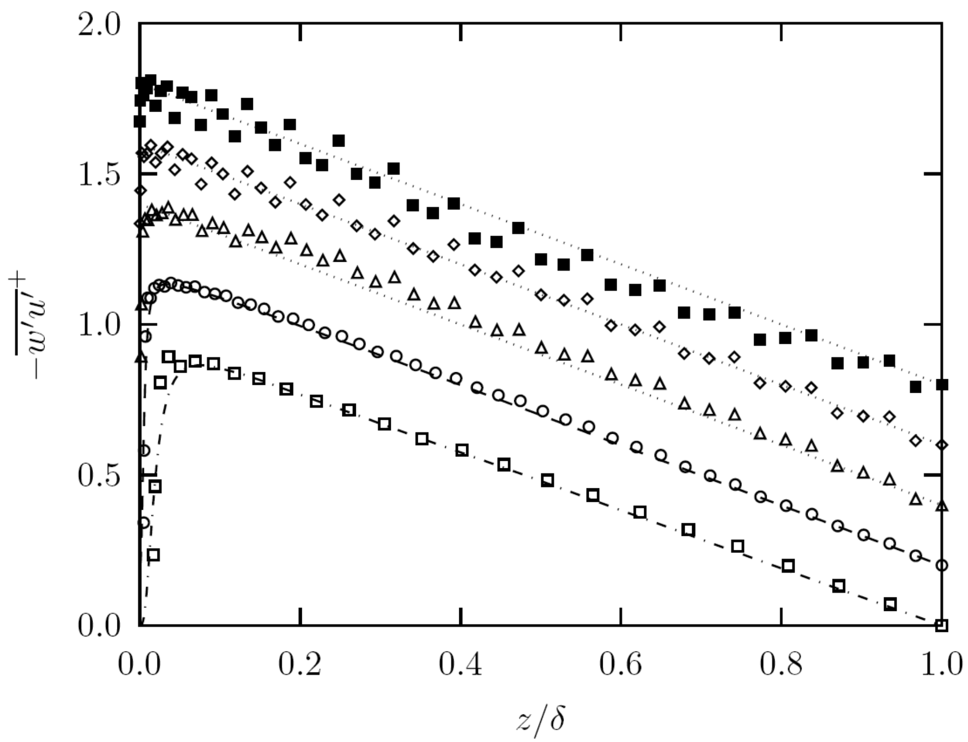

	$\mathrm{Re}_\tau = u_\tau \delta/\nu$	$\mathrm{Re} = u_{\mathrm{CL}}\delta/\nu$		$N_1 \times N_2 \times N_3$	$L_1 \times L_2$
——			$\log(z^+)/0.41 + 5.2$		
······			$1 - z/\delta$		
—·—	5.9×10^2	1.2×10^4	DNS (Moser *et al.*1999)	$384 \times 384 \times 257$	$2\pi\delta \times \pi\delta$
- - -	2.0×10^3	4.9×10^4	DNS (Hoyas & Jiménez 2006)	$6144 \times 4608 \times 633$	$8\pi\delta \times 3\pi\delta$
□	5.9×10^2	1.2×10^4	LES	$32 \times 32 \times 33$	$8\pi\delta \times 3\pi\delta$
○	2.0×10^3	4.9×10^4	LES	$64 \times 64 \times 65$	$8\pi\delta \times 3\pi\delta$
△	6.0×10^3	1.6×10^5	LES	$64 \times 64 \times 65$	$8\pi\delta \times 3\pi\delta$
◇	2.0×10^4	5.9×10^5	LES	$64 \times 64 \times 65$	$8\pi\delta \times 3\pi\delta$
■	6.0×10^4	1.9×10^6	LES	$64 \times 64 \times 65$	$8\pi\delta \times 3\pi\delta$

Reynolds stresses

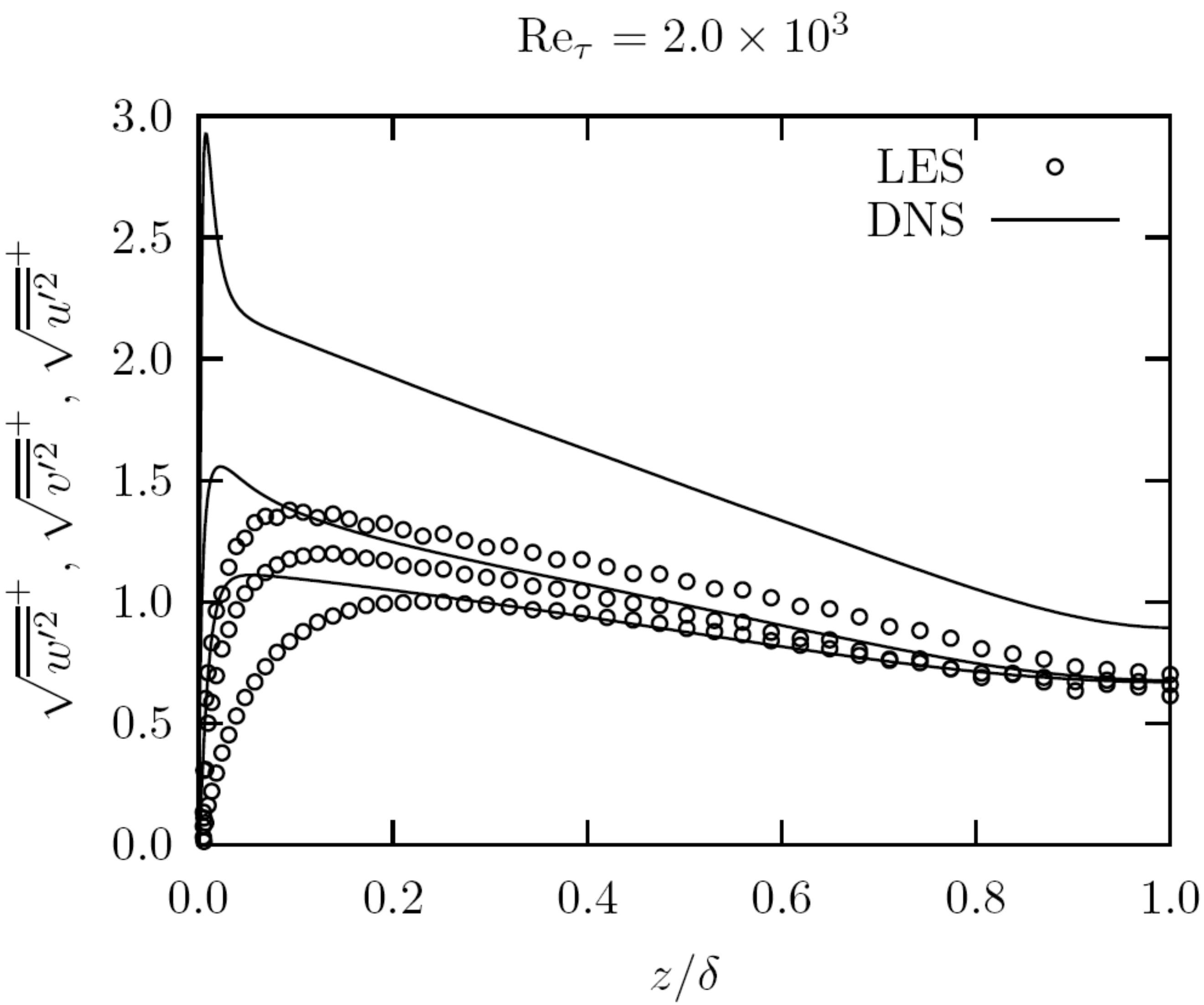

Future work

- Higher Reynolds number.
- Dynamic gamma from structure function matching.
- Application to flow over airfoil.
- Two-vortex SGS model to improve Reynolds stresses.
- Plug for related presentation:

LES of turbulent channel flow; virtual wall model

- LES of turbulent channel flow
- Turbulent flow between two parallel plates driven by pressure gradient
  - *Flow contains many features of complex wall-bounded flows*
  - *Viscous sublayer, stream-wise vortices, log layer*
- Stringent test of SGS/LES model for wall-bounded turbulence
- SGS model must accurately model turbulent transport processes
- Near-wall LES; frontier problem in present research
- Special ``virtual-wall'' near-wall SGS model
- Allow LES of wall bounded flows at large Re_tau =20,000; Re_U = 650,000
- Comparison with DNS;
- Re_tau = 590 (Moser et al, 1999
- Re_tau =2000(Hoyas et al, 2006)

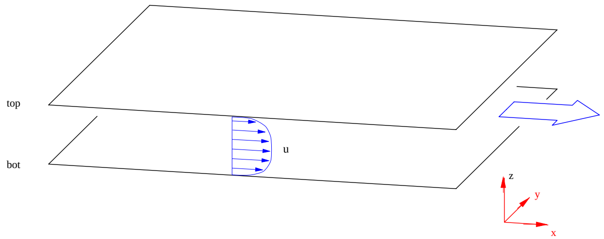

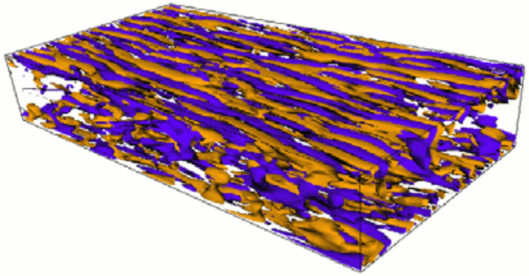

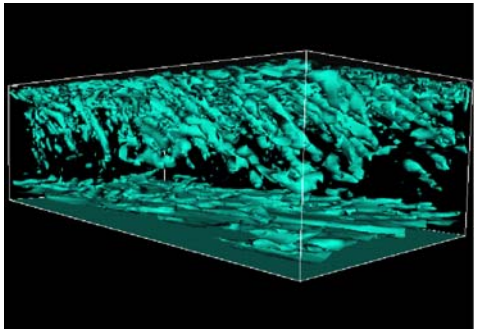

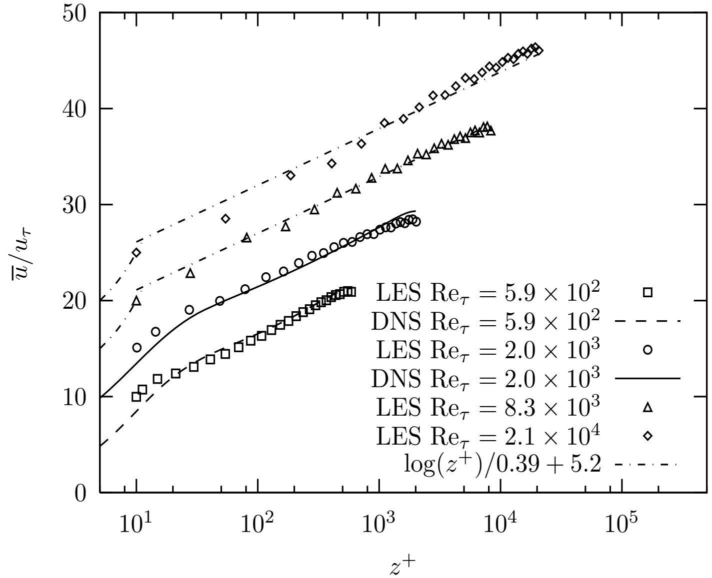

Summary

- LES methodology
  - *Two-component Favre-filtered Navier-Stokes equations*
  - *Stretched-vortex subgrid-scale (SGS) model; strucure based*
- Computational method: hybrid WENO-TCD
  - *Shock capturing low nunmerical dissipation*
  - *Verification*
    - *Decaying compressible turbulence*
    - *Riemann 1D wave (Exact Euler)*
- Large-eddy simulation of Richtmyer-Meshkov instability with reshock
  - *RM instability in plane channel with end wall; Air-SF6*
  - *Modeled on experiments of Vetter & Sturtevant (1995)*
- Traditional Statistics
  - *Mixing-layer growth*
  - *Turbulence statistics, velocity, density & scalar spectra*
- "Multi-scale modeling"
  - *Subgrid continuation statistics; spectra and anisotropy*
  - *Scalar p.d.f.s, including subgrid contribution*
  - *Effect of Schmidt number*
- Adaptive Mesh Refinement (AMROC)
  - *Berger & Colella's algorithm for conservation laws*
  - *Hierarchical data structure*
  - *WENO-TCD and stretched-vortex SGS model implemented*

Conclusions

- Large-eddy simulation of plane Richtmyer-Meshkov instability with reshock
  - *Hybrid WENO-TCD scheme with SV SGS model*
  - *Air-SF6; modeled on experiments of Vetter & Sturtevant (1995)*
- Growth of mixing-layer width
  - *Initial linear growth of interface following first shock impact*
  - *Period of nonlinear bubble/spike growth*
  - *Reshock produces rapid transition to turbulent mixing layer*
  - *Strong mixing layer growth*
  - *Enhanced by interaction with reflected expansion*
  - *Eventual saturation of growth*
- Traditional Statistics
  - *Mixing-layer growth*
  - *turbulence statistics, velocity, density & scalar spectra*
- "Multi-scale modeling"
  - *SV SGS model provides basis for subgrid continuation statistics; spectra and anisotropy*
  - *Scalar p.d.f.s, including subgrid contribution*
  - *log-dependence of scalar p.d.f. on Schmidt number*

Reynolds number and integral length

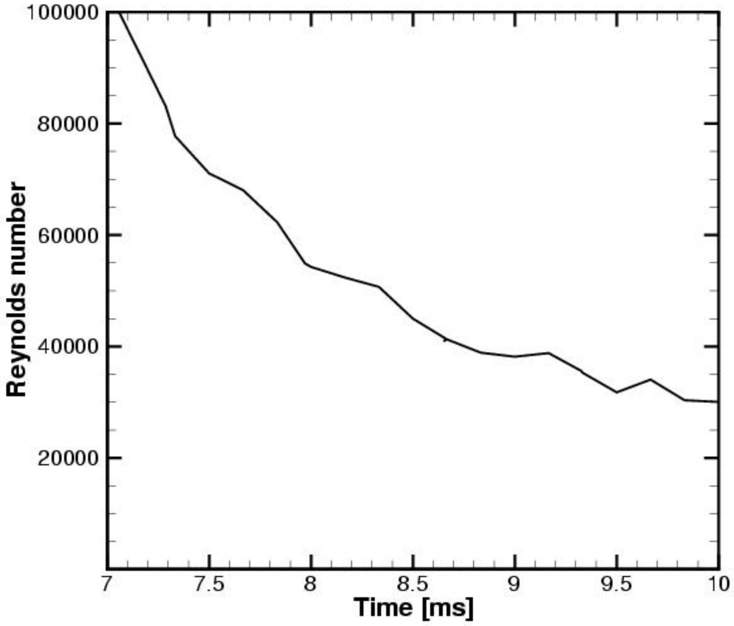

Decay on Reynolds number

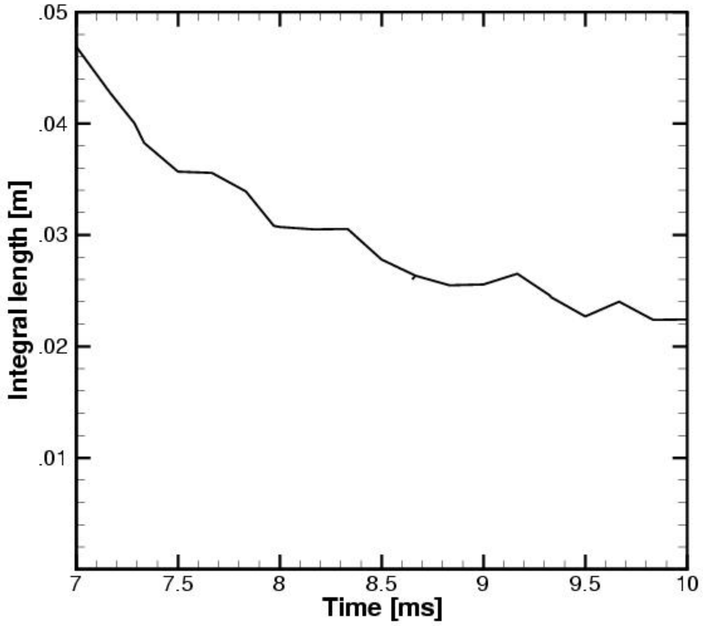

Decay of integral length

Scalar spectrum from stretched-spiral vortex

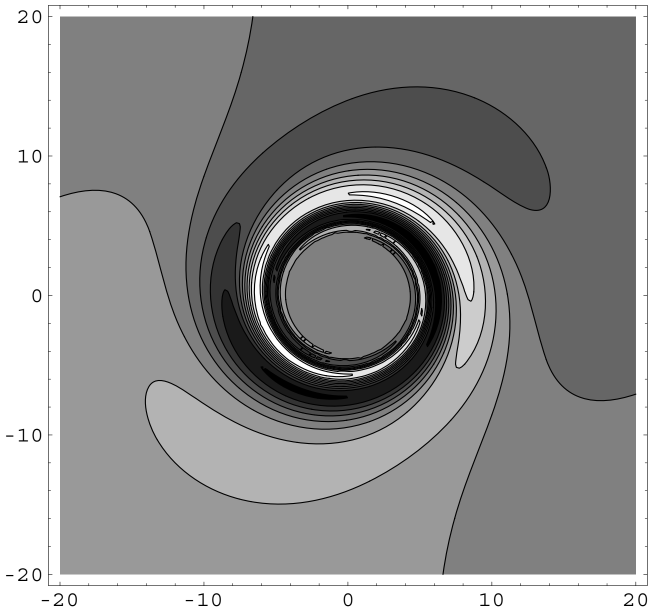

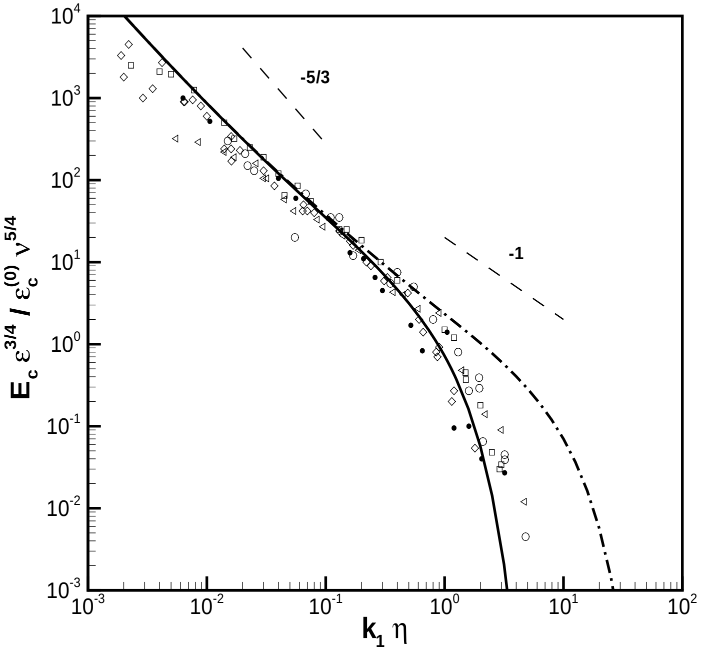

Schematic showing winding of scalar field by `subgrid vortex'. Contours of passive scalar

1-D scalar spectrum for homogeneous turbulence,Pullin & Lundgren (2001)

______ Sc = 7, ------- Sc = 700. Symbols, Data

(Gibson & Schwarz 1963)

Numerical algorithm (D. Hill, C. Pantano)

- WENO-TCD hybrid method (Hill & Pullin, JCP, 2004)
  - *Tuned-Centered Difference (TCD); away from shocks exploit smoothness of flow*
  - *Order of accuracy traded for minimization of one-step truncation error in LES equations (Ghosal, 1995)*
  - *5-point stencil -> 2-nd order accuracy*
  - *At shocks (only) revert to full WENO*
  - *Optimal WENO stencil matched to TCD stencil*
- Flux-based finite difference
  - *Naturally integrated in AMROC*
  - *Conservative, skew-symmetri*
- Skew-symmetric
  - *Energy conserving*
  - *Satisfies summation-by-parts*
- Tested in 1D, 2D, 3D
  - *Decaying compressible turbulence*
- No explicit filtering

Riemann 1D Wave

Exact solution of 1D Euler

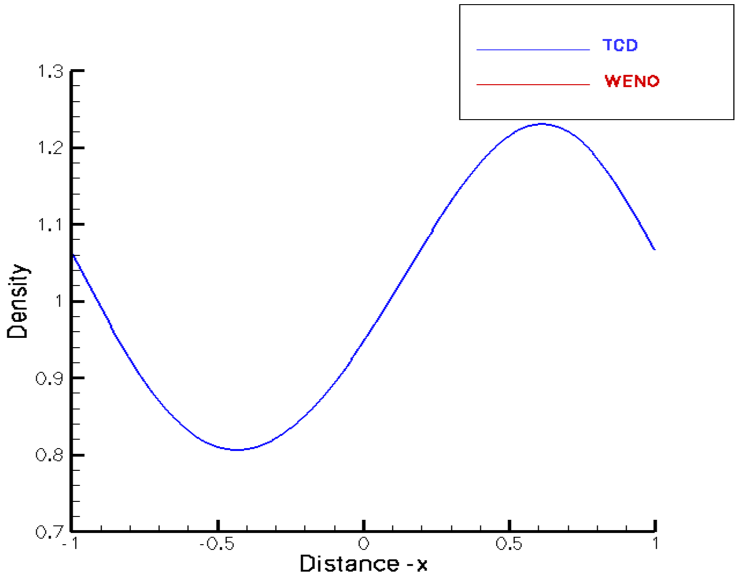

Idea: Improve K(k) for center-difference

- Finite-difference operator

$$\mathbf{D}f(x) = \frac{1}{\Delta x}\sum_{j=-3}^{j=3} d_j\,[f(x+j\,\Delta x) - f(x-j\,\Delta x)]$$

$$d_1 = \frac{2}{3}, \quad d_2 = -\frac{1}{12}, \quad d_3 = 0, \qquad \rightarrow 5-pt,\ 4^{th}\text{order}$$

$$d_1 = \frac{3}{4}, \quad d_2 = -\frac{1}{10}, \quad d_3 = -1/2, \rightarrow 7-pt,\ 6^{th}\text{order}$$

- Tuned 5-point with parameter α

$$d_1 = \frac{1}{2} - 2\alpha, \quad d_2 = \alpha, \qquad d_3 = 0, \rightarrow 5-pt,\ 2^{nd}\text{ order}$$

- Tuned 7-point with parameter α

$$d_1 = \frac{2}{3} + \alpha, \quad d_2 = -\frac{1}{12} - 4\alpha, \quad d_3 = \alpha, \rightarrow 7-pt,\ 4^{th}\text{ order}$$

Performance for LES of decaying turbulence

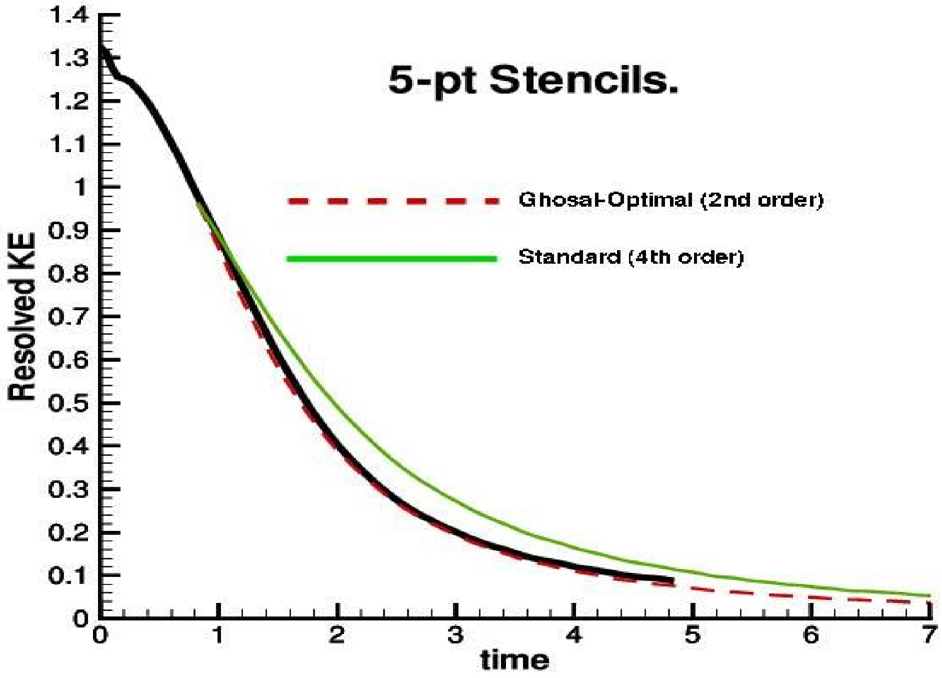

DNS and LES of Decaying compressible turbulence, M_t =0.488, R_lambda = 70.

Decay of total TKE. Black; 256^3 DNS (10-th order Pade)

Numerical algorithm (D. Hill, C. Pantano)

- WENO-TCD hybrid method (Hill & Pullin, JCP, 2004)
  - *Tuned-Centered Difference (TCD); away from shocks exploit smoothness of flow*
  - *Order of accuracy traded for minimization of one-step truncation error in LES equations (Ghosal, 1995)*
  - *5-point stencil -> 2-nd order accuracy*
  - *At shocks (only) revert to full WENO*
  - *Optimal WENO stencil matched to TCD stencil*
- Flux-based finite difference
  - *Naturally integrated in AMROC*
  - *Conservative, skew-symmetri*
- Skew-symmetric
  - *Energy conserving*
  - *Satisfies summation-by-parts*
- Tested in 1D, 2D, 3D
  - *Decaying compressible turbulence*
- No explicit filtering

Riemann 1D Wave

Exact solution of 1D Euler

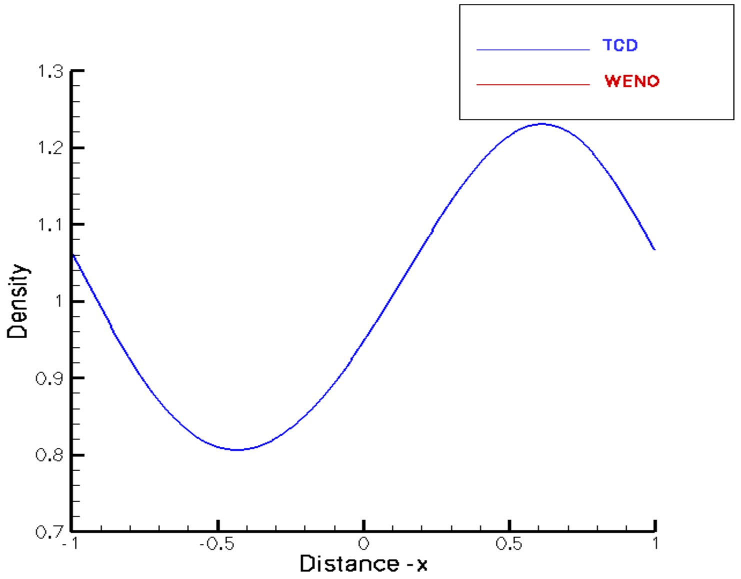

Conservation and time adaptation

- Hanging nodes exist because cells at different levels are logically conforming

- A special correction, fixup, must be applied to satisfy global conservation

- Fluxes at coarse cells next to fine cells are replaced by the sum of those fluxes at the fine cells

$$\delta \boldsymbol{F}^{1,l+1}_{i-\frac{1}{2},j} := \delta \boldsymbol{F}^{1,l+1}_{i-\frac{1}{2},j} + \frac{1}{r_{l+1}^2} \sum_{m=0}^{r_{l+1}-1} \boldsymbol{F}^{1,l+1}_{v+\frac{1}{2},w+m}(t + \kappa \Delta t_{l+1})$$

- This correction impacts the spatial as well as temporal integration scheme

$$\check{\boldsymbol{Q}}^{n+1}_{ij} := \boldsymbol{Q}^{n+1}_{ij} + \frac{\Delta t_l}{\Delta x_{1,l}} \, \delta \boldsymbol{F}^{1,l+1}_{i-\frac{1}{2},j}$$

- Ghost cell values of fine patches are obtained by linear time interpolation from the coarse patch solution

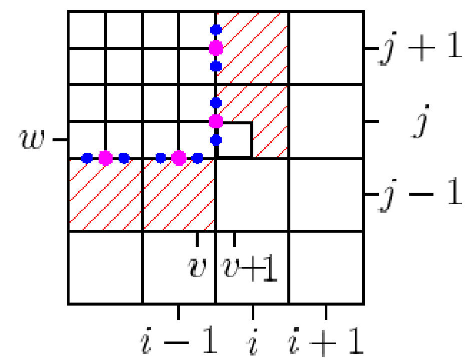

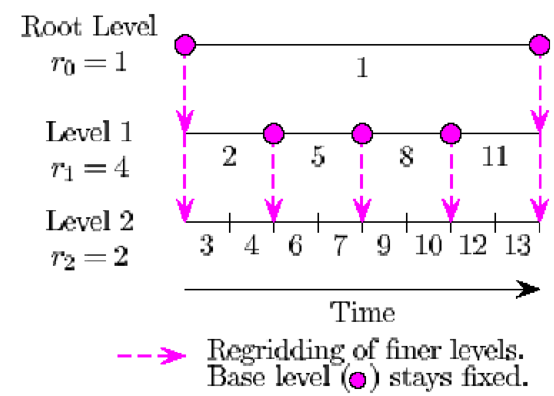

LES in the absence of strong shocks and density contacts

- The nonlinear term $\frac{\partial}{\partial x_i}\left(\rho u_i u_j\right)$ is responsible primarily for the energy cascade
- The most successful Eulerian methods are global
  - *Spectral*
  - *High-Order Pade*

- Good response across all (*spectral*) or most (*Pade*) of the resolved scales, I.e. modified wavenumber

$$\boldsymbol{F}(\partial / \partial x) = ik \qquad \boldsymbol{F}\left(D_x\right) = i\widehat{K}(k)$$

- Limitations of spectral methods:
  - *global nature results in (fatal?) ringing at discontinuities like shocks and contacts*
  - *Limited to simple geometries*

Conservation and time adaptation

- Hanging nodes exist because cells at different levels are logically conforming
- A special correction, fixup, must be applied to satisfy global conservation
- Fluxes at coarse cells next to fine cells are replaced by the sum of those fluxes at the fine cells

$$\delta \boldsymbol{F}^{1,l+1}_{i-\frac{1}{2},j} := \delta \boldsymbol{F}^{1,l+1}_{i-\frac{1}{2},j} + \frac{1}{r^2_{l+1}} \sum_{m=0}^{r_{l+1}-1} \boldsymbol{F}^{1,l+1}_{v+\frac{1}{2},w+m}(t+\kappa\Delta t_{l+1})$$

- This correction impacts the spatial as well as temporal integration scheme

$$\check{\boldsymbol{Q}}^{n+1}_{ij} := \boldsymbol{Q}^{n+1}_{ij} + \frac{\Delta t_l}{\Delta x_{1,l}}\, \delta \boldsymbol{F}^{1,l+1}_{i-\frac{1}{2},j}$$

- Ghost cell values of fine patches are obtained by linear time interpolation from the coarse patch solution

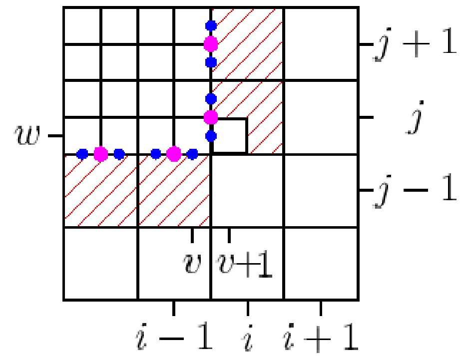

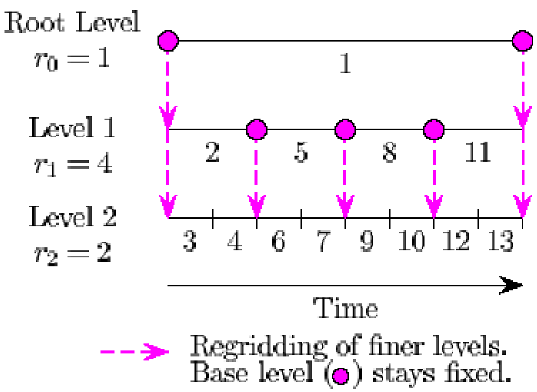

Idea: Improve K(k) for center-difference

- Finite-difference operator

$$\mathbf{D}f(x) = \frac{1}{\Delta x}\sum_{j=-3}^{j=3} d_j\,[f(x+j\,\Delta x) - f(x-j\,\Delta x)]$$

$$d_1 = \frac{2}{3}, \quad d_2 = -\frac{1}{12}, \quad d_3 = 0, \quad \rightarrow 5-pt,\ 4^{th}\text{order}$$

$$d_1 = \frac{3}{4}, \quad d_2 = -\frac{1}{10}, \quad d_3 = -1/2, \rightarrow 7-pt,\ 6^{th}\text{order}$$

- Tuned 5-point with parameter α

$$d_1 = \frac{1}{2} - 2\,\alpha, \quad d_2 = \alpha, \quad d_3 = 0, \rightarrow 5-pt,\ 2^{nd}\text{ order}$$

- Tuned 7-point with parameter α

$$d_1 = \frac{2}{3} + \alpha, \quad d_2 = -\frac{1}{12} - 4\,\alpha, \quad d_3 = \alpha, \rightarrow 7-pt,\ 4^{th}\text{ order}$$

Tuned Center-Difference Stencil (TCD)

- Error in resolved-scale energy spectrum produced by one step of Navier-Stokes equations using given discretization; Ghosal (1996)
- Asssume –
  - *Von-Karman energy spectrum*
  - *Joint normal velocty pdf*

- $\mathcal{E}^{(\mathrm{FD})}(\kappa, \tilde{\kappa}(\kappa, \alpha))$ is spectrum of truncation error for numerical method with modified wavenumber behavior $\tilde{\kappa}(\kappa, \alpha)$

- Define total discretization error;

$$\mathrm{E}_G(\alpha) = \int_0^{\frac{\pi}{\Delta x}} \mathcal{E}^{(\mathrm{FD})}(\kappa, \tilde{\kappa}(\kappa, \alpha)) d\kappa$$

Optimized 5-point TCD stencil (second order)

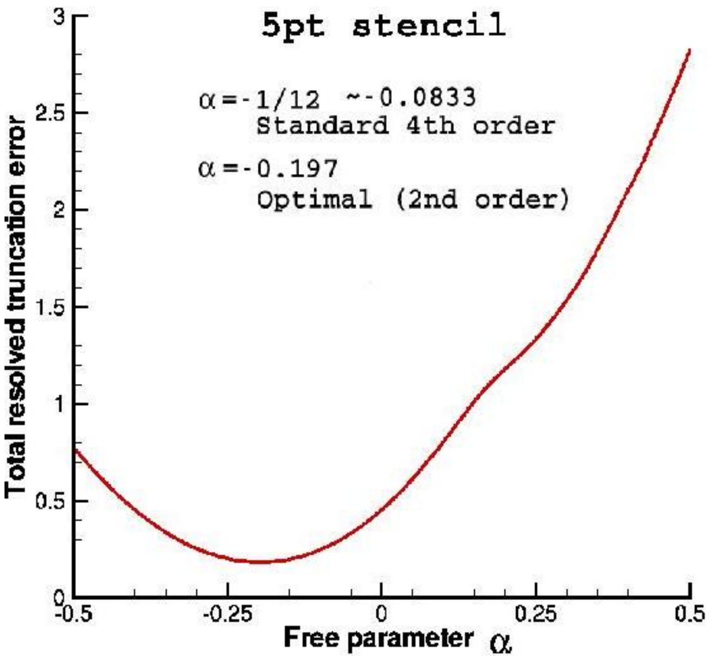

Truncation error

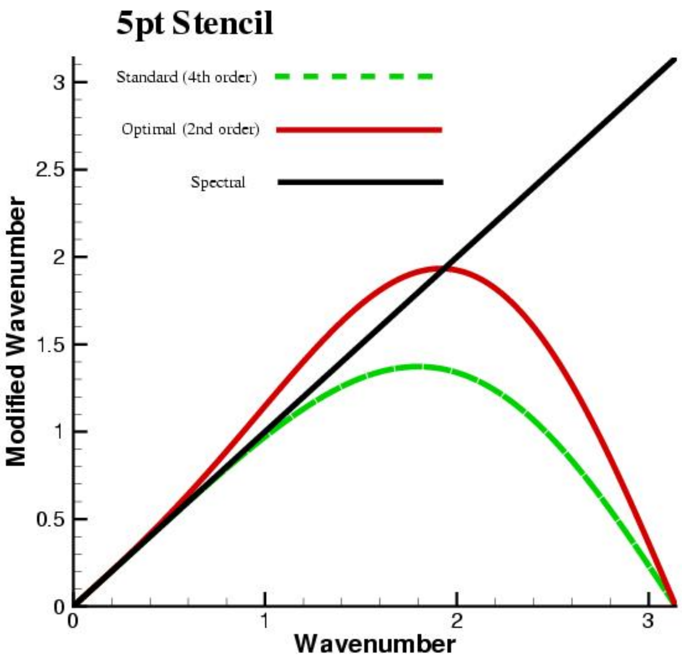

Modified wavenumber of minimal error stencil

Shock capturing solvers; WENO

- True shocks have a thickness on the mean free path order
- The shocks are not resolved: Euler equations are solved in conservative form
- Euler solver shocks are 'captured', I.e. smeared across a few cells – first-order accurate at shocks

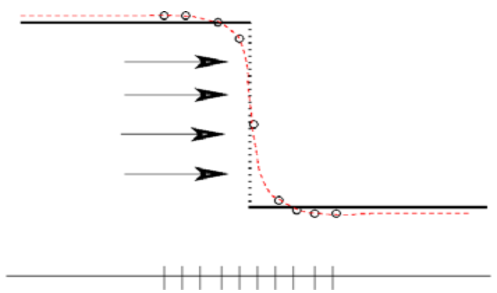

$$\frac{d\mathbf{q}}{dt}+\frac{\partial \mathbf{F(q)}}{\partial x}+\frac{\partial \mathbf{G(q)}}{\partial y}+\frac{\partial \mathbf{H(q)}}{\partial z}=0$$

$$\mathbf{q}=\left(\rho, \rho u, \rho v, \rho w, E\right)^T$$

$$\mathbf{F(q)}=\begin{pmatrix} \rho u \\ \rho u^2+P \\ \rho uv \\ \rho uw \\ \rho u(E+P) \end{pmatrix}$$

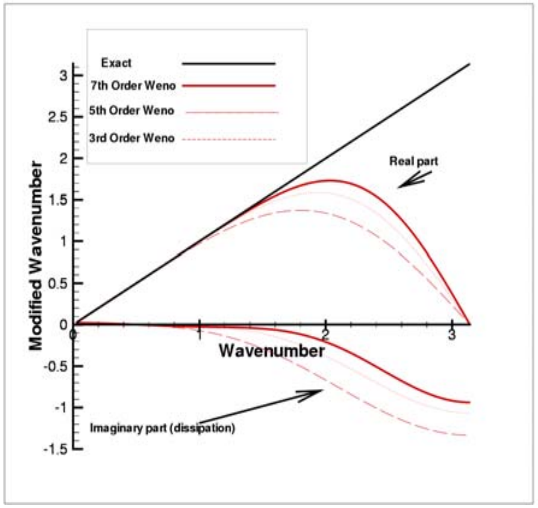

Weighted Essentially Non-Oscillatory (WENO) method (Osher)

Hybrid WENO-TCDS algorithm: LES and strong shocks (D. Hill)

- Hybrid technique: blending Weighted Essentially Non-Oscillatory (WENO) scheme with Tuned Centered-Difference (TCD) stencil.
- WENO in regions of very-large density ratio (Shocks)
  - *But WENO is not suitable for LES in smooth regions away from shocks.*
  - *Upwinding strategy is too dissipative*
- TCD stencil in smooth regions away from shocks
  - *Low numerical dissipation (centered method)*
  - *optimized for minimum resolved-scale discretization error in LES (Ghosal, 1996)*
  - *5- or 7-point stencil trades off formal order of accuracy for small dispersion errors*
- Target WENO stencil = TCD stencil
- In practice, target TCD stencil not always achieved; switch is used based on acceptable WENO smoothness measure
- Hybrid method designed for LES in presence of strong shocks

Cylindrical RM instability with AMROC (R.Deiterding)

- AMROC – Adaptive Mesh Refinement engine
- Exploratory 2D Richtmyer-Meshkov instability with reshock in wedge geometry
- Passage of the shock results in vorticity deposition by means of baroclinic generation
- Canonical model of phase 2 experiments
- Incident shock modeled by Chisnell (1998) approximation to Guderley solution for similarity shock
- Euler simulation
- Initial density interface ; sinusoidal perturbation corresponding to n = 24 on circle

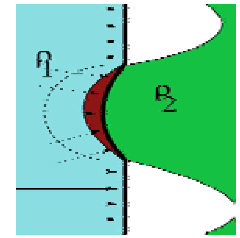

Schlieren

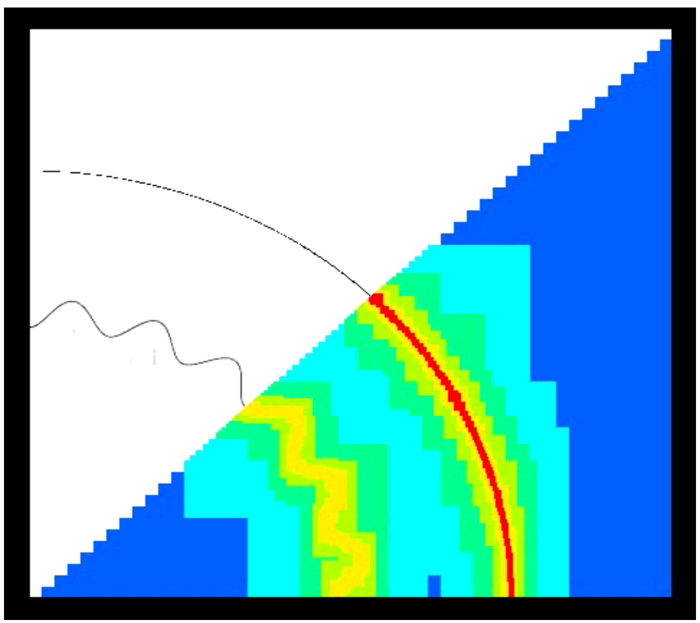

Refinement

Scalar

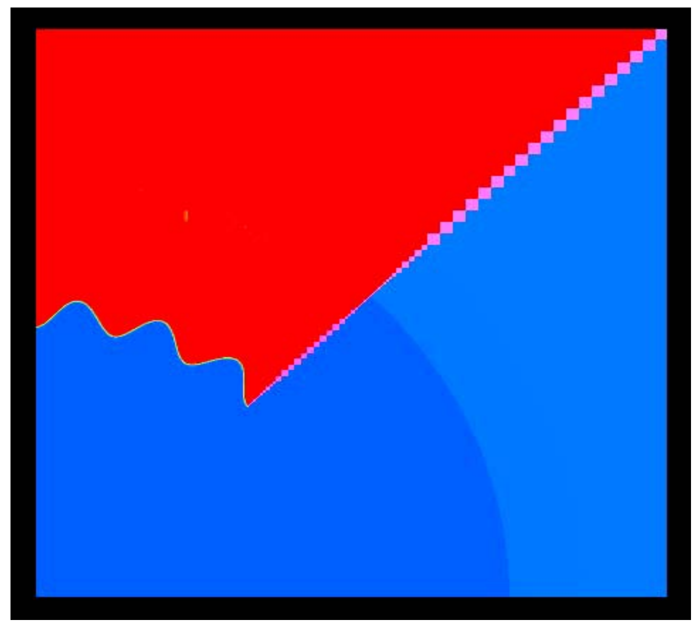

Pressure

Reacting Hydrogen Jet flame (C. Pantano)

- Planar hydrogen jet flame of Rehm & Clemens (1999), Mach=0.28
- 5 10^6 grid cells and 4 levels of refinement
- 128 processors at LLNL ALC, 50,000 cpu/hours
- Cantera chemistry solver by D. Goodwin for flamelet model

experiment

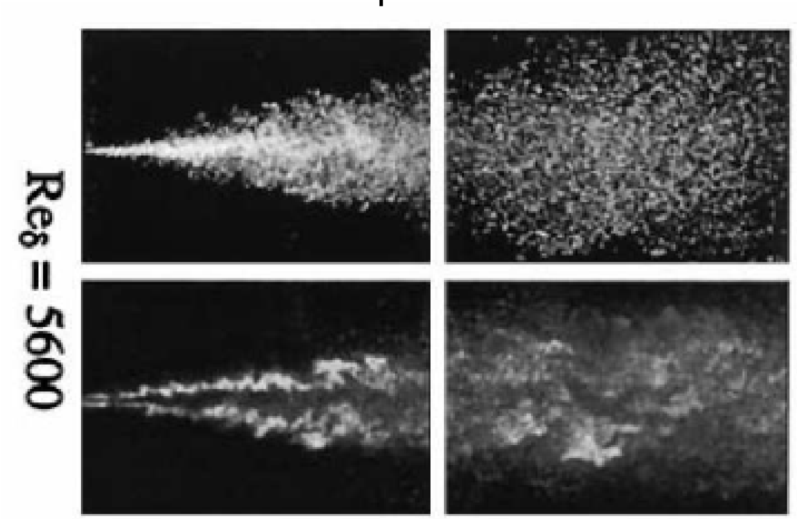

simulation